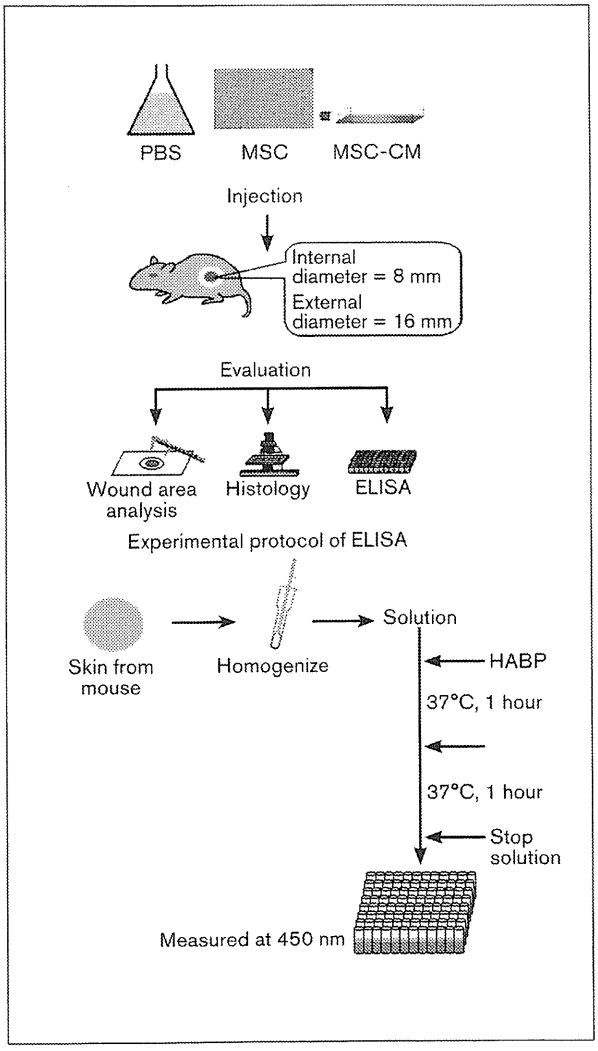

Fig 1 Scheme of the experiment.

and the quantity, proliferative capacity, and capability of differentiation of MSCs decrease with age.[8]

In general, the process of wound healing consists of inflammation, granulation, reepithelialization, and remodeling. The process also depends on various interactions between cells and extracellular matrix (ECM). Hyaluronic acid (HA), one of the components of ECM, is not solely a component of different matrices but is also involved in dynamic cellular processes in wound healing.[9–11] Therefore, it is important to observe the behavior of HA during the wound-healing process.

The present study is based on the assumption that the wound-healing accelerating effect of MSC is caused by growth factors secreted by MSCs, not by the function of the stem cells per se. The authors therefore examined the effect of MSC-conditioned medium (MSC-CM) in wound healing by using a wound-healing skin defect model and compared the effects of MSC-CM treatment with those of MSC and control (phosphate-buffered saline [PBS]) treatments. Furthermore, the amount of HA, which plays an important biologic role in skin wound healing, was measured in each group.

MATERIALS AND METHODS

Animals

Seven-week-old KSN/Slc nude mice (Chubu Kagaku Shizai) were used for the study resulting in 10 sites. Animal experimentation was conducted according to the Guidelines for Proper Conduct of Animal Experiments of the Nagoya University School of Medicine.

MSC Culture and Preparation of MSC-CM

MSCs were purchased from LONZA. Cells were cultured in Dulbecco Modified Eagle Medium (DMEM) containing a low concentration of glucose supplemented with 10% fetal bovine serum, 100 IU penicillin G, 100 μg streptomycin, and 0.25 μg amphotericin B (Sigma) at 37°C in 95% humidified air and 5% carbon dioxide.[12,13]

MSC-CM was prepared by culturing MSCs (5 × 106) using serum-free DMEM/F12 medium (Invitrogen-Gibco BRL) for 72 hours. This was centrifuged at 300×g for 5 minutes, filtrated with a 0.22-μm syringe filter, and then used for the experiment.[14]

Wound-Healing Model, Cell Transplantation, and Administration of Test Materials

The experimental protocol is shown in Fig 1. The animals were randomly divided into three groups: control group, which would receive an injection of PBS; the MSC transplantation group; and the MSC-CM administration group. An excisional wound-splinting model that was established in a previous report was used.[15] In brief, two 8-mm full-thickness excisional skin wounds were formed on both sides of the midline on the back of a mouse. Doughnut-shaped silicone splints were placed on each wound so that the wound was at the center of the splint. Instant adhesive (Krazy Glue) was used to glue the splints to the skin, and the splint was then sutured to secure it.

For animals in the MSC transplantation group, PBS containing 4 × 106 cells (80 μL) was injected into four spots around each wound, PBS containing 1 × 106 cells (20 μL) was placed on the wound, and Tegaderm (3M) was placed on the wound. For the MSC-CM and control groups, 20 μL of MSC-CM or PBS (control) was injected in four spots around the wound and placed on the wound in the same manner as the MSC transplantation group.

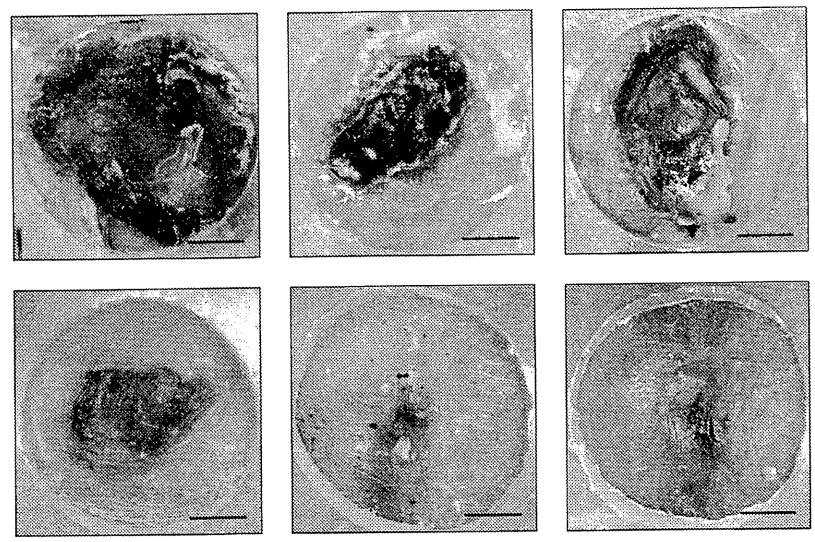

Fig 2 Macroscopic findings at 7 and 14 days after injection. *(Upper row)* 7 days after administration; *(bottom row)* 14 days after administration. *(Left column)* Control group; *(middle column)* MSC group; *(right column)* MSC-CM group. Bar = 2 mm.

Assessment of Wound Area

Digital photographs of the wounds were taken on the day of administration and on 3, 5, 7, 10, and 14 days after administration. The area of the wound was measured using an image analysis program (Scion Image, Scion). The percentage of the area of wound was evaluated with the formula (area of actual wound/area of original wound) × 100.

Mice were sacrificed at 7 and 14 days after administration of test materials. Samples were prepared for histologic and immunologic analyses and evaluated using the image analysis program.

Histologic Examination and Immunofluorescent Staining

Extracted tissue was fixed with 4% paraformaldehyde and embedded into OCT compound (Tissue-Tek, Miles). The samples were sliced into 5-μm sections and stained with hematoxylin-eosin. The expression of HA was confirmed with immunostaining (Rockland Immunochemicals) as follows. First, biotinylated HA binding protein (Seikagaku) was diluted 1:100 with PBS and incubated on slides with the samples at room temperature for 2 hours. Then, the slides were rinsed with PBS and incubated with fluorescein isothiocyanate–conjugated streptavidin (Beckman Coulter) diluted 1:200 with PBS at room temperature for 15 minutes. The slides were sealed with a mounting medium containing 4,6-diamidino-2-phenylindole-2-HCl (DAPI) (Vector Laboratories). To reduce intrinsic fluorescence in the tissue, the slide was incubated with 1% bovine serum albumin for 1 hour and then incubated with a streptavidin-biotin blocking kit (Vector Laboratories) at room temperature for 20 minutes to block endogenous biotin. Then, the tissue and immunofluorescence were observed with a fluorescence microscope (Microscope BX51; Olympus).

Enzyme-Linked Immunosorbent Assay of HA

An enzyme-linked immunosorbent assay (ELISA) HA quantitative test kit (Seikagaku) was used according to the provided protocol to determine the amount of HA in samples collected at 7 and 14 days after administration (Fig 1). The HA test kit is an enzyme-binding protein assay kit using a capture molecule known as HA binding protein (HABP). The samples are first reacted with biotinylated HABP solution and then with horseradish peroxidase–labeled streptavidin solution as the secondary reaction. The reaction is stopped with stop solution, and the amount of HA is colorimetrically measured at 450 nm. HA levels of all samples were calculated with reference to readings of blanks and a reference solution supplied with the kit.

Statistical Analysis

Differences between the groups were evaluated with the Tukey-Kramer test using one-way analysis of variance. A value of $P < .05$ was considered to indicate statistical significance.

RESULTS

Macroscopic Observation of Wound Healing

The wounds on the mice were observed macroscopically at 3, 5, 7, 10, and 14 days after surgery, and tissues were collected at days 7 and 14. At 7 days, healing of the wound was incomplete in all groups (Fig 2). The surface of the wound had not epithelialized macroscopically, especially in the control group. Exudate was

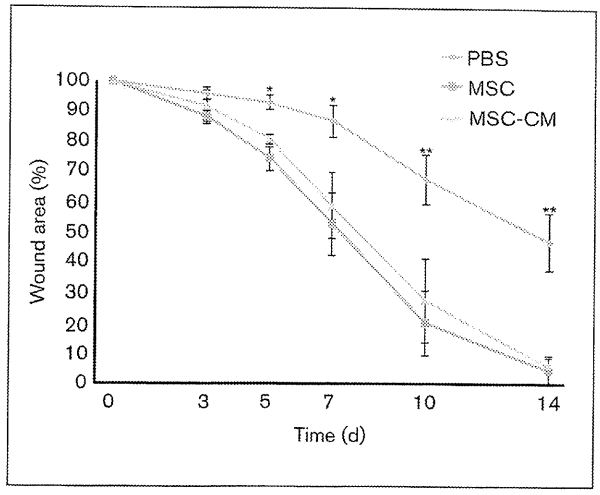

Fig 3 Time-dependent changes in the wound area determined with image analysis software (area of actual wound/area of original wound × 100). MSC-CM versus control: $^{*}P < .05$; $^{**}P < .01$.

observed in all groups. At 14 days, epithelialization appeared to be nearly complete in the MSC and MSC-CM groups, but the wounds were not completely closed in the control group (Fig 2). Changes in the wound area percentages at 7 and 14 days, as calculated with digital image analysis software, were as follows: 88.48% ± 3.49% and 42.64% ± 5.36% in the control group, 46.41% ± 5.49% and 4.90% ± 2.36% in the MSC group, and 47.77% ± 4.86% and 5.74% ± 2.85% in the MSC-CM group, respectively (Fig 3).

An acceleration of wound healing was observed in the MSC and MSC-CM groups as compared to the control group. At 5 days and later, there was a statistically significant difference in the wound area between the MSC and MSC-CM groups and the control group ($P < .05$, Fig 3); however, there were no significant differences between the MSC and MSC-CM groups.

Histopathologic Observations

At 7 days after surgery, inflammatory cells were observed in all groups. The epidermis of the wound was affected, especially in the control group. In the MSC and MSC-CM groups, epithelialization was advanced, and thick granulation tissue was observed (Fig 4).

At 14 days after wound creation and administration of the test materials, the number of inflammatory cells was decreased compared to 7 days. Reepithelialization was observed in the MSC and MSC-CM groups. Fluorescence microscopy showed decreases in HA production in all groups as compared to 7 days (Fig 5).

HA Production

The mean amounts of HA at 7 and 14 days were 1,512.0 ± 84.10 ng/mg and 683.7 ± 56.4 ng/mg in the control group, 2,450.3 ± 225.7 ng/mg and 1,690.2 ± 170.2 ng/mg in the MSC group, and 2,360.6 ± 230.0 ng/mg and 1,570.1 ± 142.5 ng/mg in the MSC-CM group, respectively. HA production in the MSC and MSC-CM groups at 7 and 14 days was significantly increased versus the control group. There were no statistically significant differences between the MSC and MSC-CM groups (Figs 6 and 7).

DISCUSSION

It is difficult to heal chronic wounds, and little improvement has been seen in the prevalence of complications and prevention of lesions in the past decade.[16] Even the most effective therapy for chronic wound repair has a healing rate of only 50%. In the present study, the area of the wound had shrunk by about 50% in the control group after 14 days. Therefore, an innovative therapy to accelerate wound healing and regeneration is needed. A major goal in wound healing is to discover methods to induce repair of the damaged site on the skin as completely as possible.[17] The present study revealed that MSC and MSC-CM can accelerate granulation and reepithelialization of wounds and demonstrated that these phenomena have a relationship with ECM, including HA.

The effect of this therapy on wound healing was examined using an excisional wound-splinting mouse model that prevents natural repair as a result of contracture of the skin; this allowed observation of granulation tissue and reepithelialization. The results indicated that closure of wounds in the control group was delayed significantly in comparison to the MSC and MSC-CM groups. In the MSC and MSC-CM groups, there were significant differences at 6 days and later as compared to the control group. To the best of the authors' knowledge, there are few reports

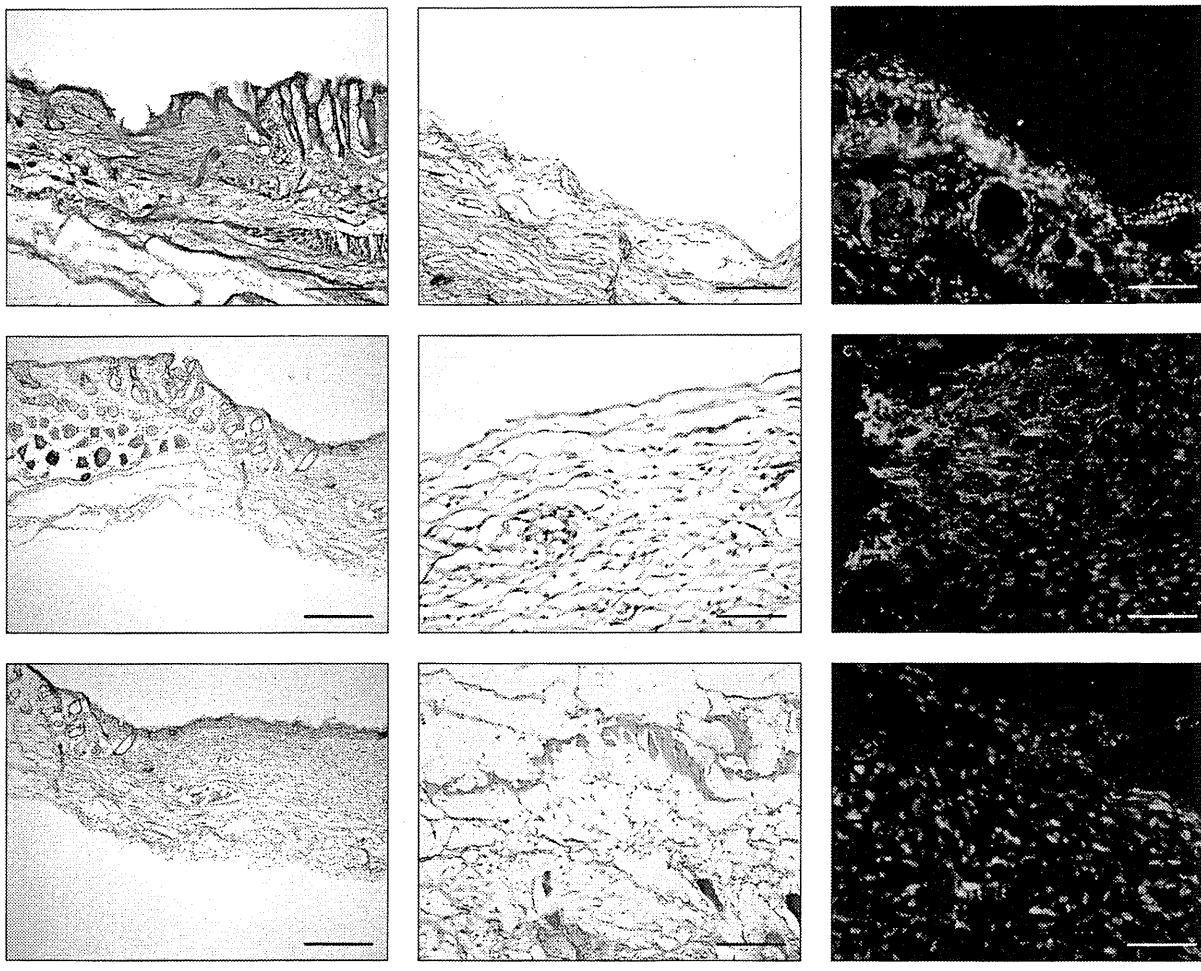

Fig 4 Histologic findings at 7 days after administration. Left and middle columns: hematoxylin-eosin staining; right column: immunostaining with HA. Blue, red, and green signals represent nuclei stained with DAPI, transplanted MSC, and HA, respectively. Top row: control group; middle row: MSC group; bottom row: MSC-CM group. Bar = 3 mm for left column; bar = 25 μm for center and right columns.

of culture supernatants of MSCs promoting wound healing, although many studies have demonstrated that MSC has a wound-healing effect. Ueda and Nishino[14] showed that CM of primary tooth stem cells was effective in improving ultraviolet-irradiated mouse skin tissue. This is the first experiment to show that CM can accelerate wound healing, even in a skin defect. It was already known that MSC-CM has effects on proliferation and migration of epithelium in vitro. Therefore, it was hypothesized that administration of MSC-CM to a wound might influence the epidermis and epidermal appendages, and thus regeneration of the epidermis. In a previous study, most MSCs remained at 7 days after surgery, and the number of MSCs was lower by 14 days.[18] The findings of this study correspond to these results. The amount of HA was reduced at 14 days as compared to that seen at 7 days. The mechanism that contributes to these phenomena is still not entirely clear. In the process of wound healing, cytokine and ECM molecules play favorable roles in epithelialization. Accordingly, the amount of HA was decreased because epithelialization of the skin was accelerated by the injected MSC and MSC-CM, and HA completed its role in this process. It was reported in a recent study that a peak of HA expression appeared at 7 days.[19] This study also confirmed expression of HA. HA plays an important role in the proliferation and migration of keratinocytes.[9–11] These results suggest that HA is important for the reepithelialization process and also helps reduce deposits of collagen and scars.[20]

Treatment using MSCs is effective; however, their numbers, proliferative capacity, and differentiation capability decrease with aging.[8] However, MSC-CM

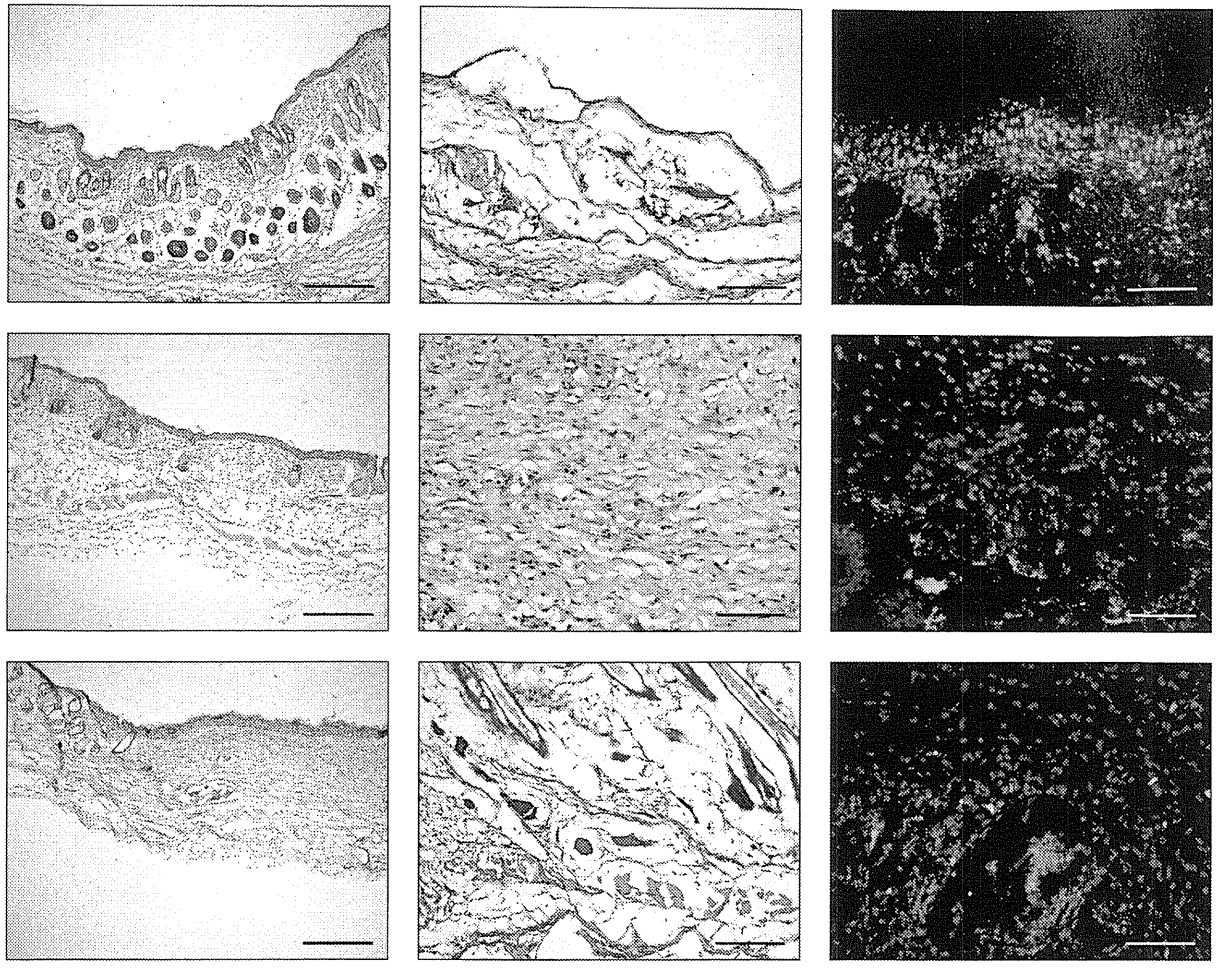

Fig 5 Histologic findings at 14 days after administration. Left and middle columns: hematoxylin-eosin staining; right column: immunostaining with HA. Blue, red, and green signals represent nuclei stained with DAPI, transplanted MSC, and HA, respectively. Top row: control group; middle row: MSC group; bottom row: MSC-CM group. Bar = 3 mm for left column; bar = 25 μm for center and right columns.

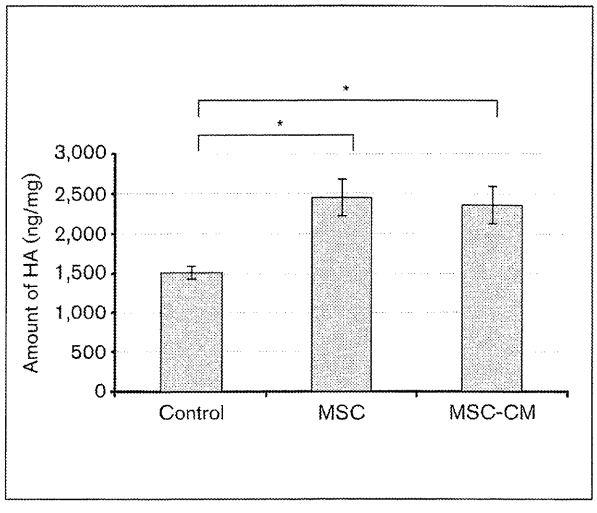

Fig 6 HA production at 7 days after administration, as determined with ELISA. *$P < .05$.

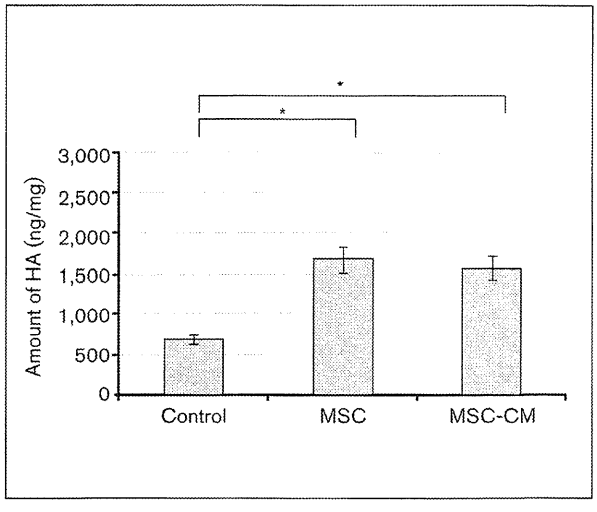

Fig 7 HA production at 14 days after administration, as determined with ELISA. *$P < .05$.

is obtained from an incubation process of the cells, and it is often discarded. This experiment showed that MSC and MSC-CM groups accelerated wound healing versus an untreated control group. The MSC-CM group showed wound healing comparable to that of the MSC group. There are the following advantages with the use of MSC-CM as compared with MSCs: *(1)* The risk of tumorigenesis is reduced because no stem cells are transplanted, and *(2)* no large-scale facilities, management expenses, or complicated processes to culture living stem cells are required. For example, freeze-dried CM can be prepared as a drug formulation. The authors consider that MSC-CM can be effective as a new treatment for wound-healing therapy for the skin as an alternative to stem cell transplantation.

ACKNOWLEDGMENTS

The authors wish to thank Naomi Nishio, Ken-ichi Isobe, and members of the Department of Oral and Maxillofacial Surgery, Nagoya University Graduate School of Medicine, for their generous assistance and contributions to this study.

REFERENCES

1. Liechty KW, Sablich TJ, Adzick NS, Crombleholme TM. Recombinant adenoviral mediated gene transfer in ischemic impaired wound healing. Wound Repair Regen 1999;7: 148–153.
2. Strecker-McGraw MK, Jones TR, Baer DG. Soft tissue wounds and principles of healing. Emerg Med Clin North Am 2007;25:1–22.
3. Page JC. Critiquing clinical research of new technologies for diabetic foot wound management. J Foot Ankle Surg 2002;41: 251–259.
4. Li H, Fu X, Ouyang Y, Cai C, Wang J, Sun T. Adult bone-marrow-derived mesenchymal stem cells contribute to wound healing of skin appendages. Cell Tissue Res 2006;326: 725–736.
5. Le Pillouer-Prost A. Fibroblasts. What's new in cellular biology? J Cosmet Laser Ther 2003;5:232–238.
6. Satoh H, Kishi K, Tanaka T, et al. Transplanted mesenchymal stem cells are effective for skin regeneration in acute cutaneous wounds. Cell Transplant 2004;13:405–412.
7. Pittenger MF, Mackay AM, Beck SC, et al. Multilineage potential of adult human mesenchymal stem cells. Science 1999;284:143–147.
8. Kern S, Eichler H, Stoeve J, Kluter H, Bieback K. Comparative analysis of mesenchymal stem cells from bone marrow, umbilical cord blood, or adipose tissue. Stem Cells 2006;24: 1294–1301.
9. Yamada Y, Itano N, Hata K, Ueda M, Kimata K. Differential regulation by IL-1beta and EGF of expression of three different hyaluronan synthases in oral mucosal epithelial cells and fibroblasts and dermal fibroblasts: Quantitative analysis using real-time RT-PCR. J Invest Dermatol 2004;122:631–639.
10. Tammi R, Ripellino JA, Margolis RU, Tammi M. Localization of epidermal hyaluronic acid using the hyaluronate binding region of cartilage proteoglycan as a specific probe. J Invest Dermatol 1988;90:412–414.
11. Tammi R, Ripellino JA, Margolis RU, Maibach HI, Tammi M. Hyaluronate accumulation in human epidermis treated with retinoic acid in skin organ culture. J Invest Dermatol 1989;92: 326–332.
12. Gronthos S, Brahim J, Li W, et al. Stem cell properties of human dental pulp stem cells. J Dent Res 2002;81:531–535.
13. Miura M, Gronthos S, Zhao M, et al. SHED: Stem cells from human exfoliated deciduous teeth. Proc Natl Acad Sci USA 2003;100:5807–5812.
14. Ueda M, Nishino Y. Cell-based cytokine therapy for skin rejuvenation. J Craniofac Surg 2010;21:1861–1866.
15. Galiano RD, Michaels J, Dobryansky M, Levine JP, Gurtner GC. Quantitative and reproducible murine model of excisional wound healing. Wound Repair Regen 2004;12:485–492.
16. Boulton AJ, Vileikyte L, Ragnarson-Tennvall G, Apelqvist J. The global burden of diabetic foot disease. Lancet 2005; 366:1719–1724.
17. Martin P. Wound healing—Aiming for perfect skin regeneration. Science 1997;276:75–81.
18. Nishino Y, Yamada Y, Ebisawa K, et al. Stem cells from human exfoliated deciduous teeth (SHED) enhance wound healing and possibility of novel cell therapy. Cytotherapy 2011;13: 598–605.
19. Dechert TA, Ducale AE, Ward SI, Yager DR. Hyaluronan in human acute and chronic dermal wounds. Wound Repair Regen 2006;14:252–258.
20. Longaker MT, Chiu ES, Adzick NS, Stern M, Harrison MR, Stern R. Studies in fetal wound healing. V. A prolonged presence of hyaluronic acid characterizes fetal wound fluid. Ann Surg 1991;213:292–296.

Human Deciduous Teeth Dental Pulp Cells With Basic Fibroblast Growth Factor Enhance Wound Healing of Skin Defect

Yudai Nishino, DDS, Katsumi Ebisawa, MD, PhD,*† Yoichi Yamada, DDS, PhD,‡ Kazuto Okabe, DDS, PhD,* Yuzuru Kamei, MD, PhD,† and Minoru Ueda, DDS, PhD**

Abstract: In this research, we examined the effect on wound healing applying basic fibroblast growth factor (b-FGF) that is approved for clinical use to enhance wound healing and human deciduous teeth dental pulp cells (hDPCs) in clinics, but that have been attracting attention as a novel stem cell source in recent years. Human deciduous teeth were harvested from healthy volunteers, and hDPCs were isolated. We used a nude mouse full-thickness skin defect model and evaluated wound healing by macroscopic view and histologic and histomorphometric analysis. The mice were randomly divided into 4 groups: phosphate-buffered saline–treated group (control group), b-FGF–treated group (b-FGF group), hDPC-treated group (hDPC group), and hDPC and b-FGF–treated group (hDPC/b-FGF group). Basic fibroblast growth factor and hDPC groups accelerated wound healing compared with the control group. There was no statistically significant difference in wound healing observed between the hDPC and b-FGF groups. The hDPC/b-FGF group demonstrated accelerated wound healing compared with other groups. At day 14, PKH26-positive cells were surrounded by human type I collagen in hDPC and hDPC/b-FGF groups in immunohistologic evaluation. Significantly increased collagen fibril areas in wound tissues were observed in b-FGF, hDPC, and hDPC/b-FGF groups as compared with the control group at days 7 and 14. Our results showed that the hDPC/b-FGF group significantly promotes wound healing compared with other groups. This study implies that deciduous teeth that are currently considered as medical spare parts might offer a unique stem cell resource for potential of new cell therapies for wound healing in combination with b-FGF.

From the Departments of *Oral and Maxillofacial Surgery and †Plastic and Reconstructive Surgery, Nagoya University Graduate School of Medicine; and ‡Center for Genetic and Regenerative Medicine, Nagoya University School of Medicine, Nagoya, Japan.

Received May 31, 2010.
Accepted for publication August 2, 2010.

Address correspondence and reprint requests to Katsumi Ebisawa, MD, PhD, Department of Plastic and Reconstructive Surgery, Nagoya University Graduate School of Medicine, 65 Tsurumai-cho, Showa-ku, Nagoya 466-8550, Japan; E-mail: ebisawa@med.nagoya-u.ac.jp

This work was partly supported by the Japan Society for the Promotion of Science (KAKENHI, 20592326).
The authors report no conflicts of interest.

Copyright © 2011 by Mutaz B. Habal, MD

ISSN: 1049-2275
DOI: 10.1097/SCS.0b013e318207b507

Key Words: Human deciduous teeth dental pulp cells, basic fibroblast growth factor, wound healing, cell transplantation

(*J Craniofac Surg* 2011;22: 438–442)

Wound healing is a complex phenomenon that involves sequential phases that overlap in time and space, interact, and affect each other dynamically both at the gene and protein levels. It is difficult to control wound healing after tumor excision, cleft lip, and trauma in the craniofacial area. In case of intractable ulcers, keloids, and hypertrophic scars, wound healing is extremely stressful on patients.[1] A lot of treatment methods have been examined; however, there is no one established, acceptable method. A new treatment modality needs to be established.

Regenerative medicine is a promising tool in a new clinical platform for a whole spectrum of intractable diseases. Various stem cells have been reported, especially mesenchymal stem cells (MSCs) isolated from various tissues including bone marrow, adipose tissue, skin, umbilical cord, and placenta, and used in clinical applications in skin regeneration.[2–5] They promote wound healing and may reduce scars.[6] There are several lines of evidence that reported that MSCs have been applied to accelerate wound healing through differentiation and paracrine effects.[6,7] Mesenchymal stem cells, referred to as stromal progenitor cells, are self-renewing and expandable stem cells. However, bone marrow aspiration is an invasive procedure for the donor. In addition, the number, proliferation, and differentiation potential of MSCs decline with increasing age.[8]

Dental pulp appears to be an alternate and more readily available source of stem cells in the craniofacial area. Stem cells from the deciduous teeth dental pulp have been identified as a novel population of stem cells that have the capacity of self-renewal and multilineage differentiation similar to MSCs.[9,10] They have also been reported to have the potential for use in cell-based therapy for systemic disease, such as neurologic disease and cardiac disease, and to ameliorate ischemic disease.[11–13] To date, there is no report of them having been used in wound healing.

Basic fibroblast growth factor (b-FGF) was approved for clinical use in Japan in 2001 and has been used clinically in recent years. Fibroblast growth factors have been shown to have profound effects on various cell types, influencing their proliferation, differentiation, and other functions.[14–16] Basic fibroblast growth factor is one of the fibroblast growth factor families of single-chain polypeptides (14 ± 18 kd) that regulates the development and maintenance of the cellular derivatives of mesoderm and neuroectoderm. Of all known growth factors, b-FGF probably has the broadest range of target cells, including essentially all of the diverse cells involved in wound healing.[17] Basic fibroblast growth factor is noted for its noninvasive approach.

Copyright © 2011 Mutaz B. Habal, MD. Unauthorized reproduction of this article is prohibited.

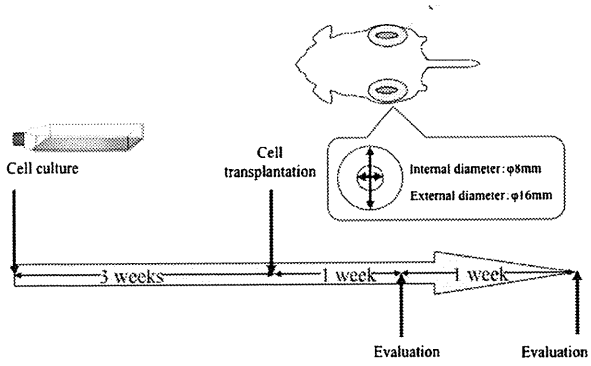

FIGURE 1. Scheme of experimental protocol.

In this research, we examined the effect of applying b-FGF on wound healing, which has already been used in clinical applications, and human deciduous teeth dental pulp cells (hDPCs). These results may provide us with new information of cell therapies for wound healing in conjunction with b-FGF.

MATERIALS AND METHODS

Animals

Seven-week-old KSN/Slc nude mice, obtained from the Chubu Kagaku Shizai Corporation (Nagoya, Japan), were used. The animal experiments were performed in accordance with the Guidelines for Animal Experimentation of Nagoya University School of Medicine.

Cell Culture of hDPCs

The experimental protocol is summarized (Fig. 1). Human deciduous teeth dental pulp cells were obtained from clinically healthy extracted deciduous teeth from 7- to 8-year-old children. The ethics committee of Nagoya University approved our experimental protocols. Human deciduous teeth dental pulp cells were isolated and cultured as previously described.[9,10] Briefly, the pulp was gently removed and digested in a solution of 3 mg/mL collagenase type I and 4 mg/mL dispase for 1 hour at 37°C. Cells were cultured in conditioned medium consisting of low-glucose Dulbecco's modified Eagle medium with growth supplements (50 mL of fetal bovine serum, 10 mL of 200-mmol/L L-glutamine, and 0.5 mL of penicillin-streptomycin mixture containing 25 U of penicillin and 25 kg of streptomycin [Lonza, Inc, Walkersville, MD]) at 37°C in a humidified atmosphere containing 95% air and 5% CO_2. The medium was changed every 3 days. When the cells were confluent, they were passaged. Cells up to 5 passages were used in this experiment.

Basic Fibroblast Growth Factor

Recombinant human b-FGF (Kaken Pharmaceutical Co, Ltd, Tokyo, Japan) was dissolved in phosphate-buffered saline (PBS) before use. The concentration of b-FGF (100 μg/mL) was according to the manufacturer's instructions.

Wound Healing Model

The excisional wound splint model was used as described previously.[18] Mice were individually anesthetized, and two 8-mm full-thickness skin defects were created on the dorsal surface each side of the midline. A doughnut-shaped silastic splint was placed so that the wound was centered within the splint. A fast-bonding adhesive (Krazy Glue, Columbus, OH) was used to fix the splint to the skin, followed by interrupted 4-0 silk sutures to stabilize its position.

Cell Transplantation

The cultured hDPCs were detached from culture dishes by enzymatic treatment with 0.05% trypsin/EDTA. Human deciduous teeth dental pulp cells labeled with PKH26 (Sigma-Aldrich, St Louis, MO) were then prepared. The animals were randomly divided into 4 groups: 100 μL of PBS was applied to the wound bed (control group), 100 μL of 100 μg/mL b-FGF solution was applied in the b-FGF group, 5×10^6 cells of hDPCs suspended with 100 μL of PBS was applied in the hDPC group, and 5×10^6 cells of hDPCs suspended with 100 μL of 100 μg/mL b-FGF solution was applied in the hDPC/b-FGF group. Tegaderm (3M, London, Ontario, Canada) was placed over the wounds. The animals were housed individually.

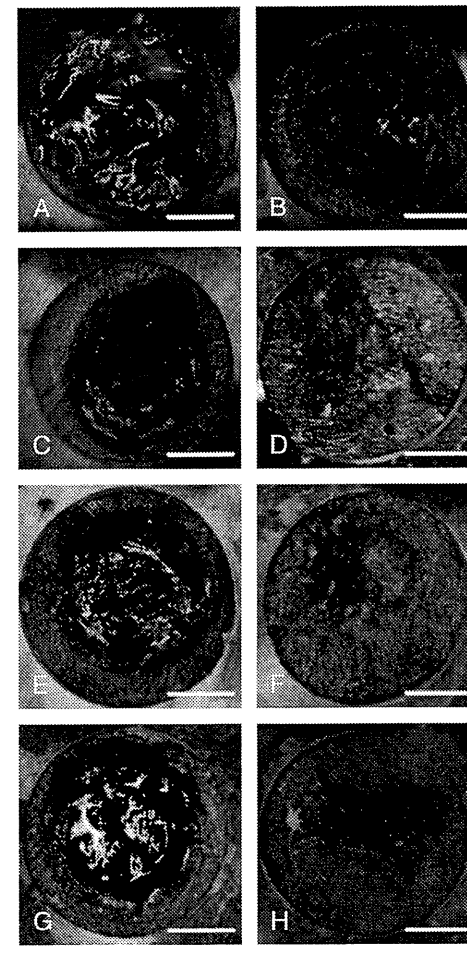

FIGURE 2. Macroscopic observations of the wounds at days 7 and 14 after the procedure. Left panel (A, C, E, G) shows day 7; right panel (B, D, F, H) shows day 14. A and B show results from the control group; C and D show results from the b-FGF group; E and F show results from the hDPC group; and G and H show results from the hDPC/b-FGF group, respectively. Bars = 3 mm.

© 2011 Mutaz B. Habal, MD

Copyright © 2011 Mutaz B. Habal, MD. Unauthorized reproduction of this article is prohibited.

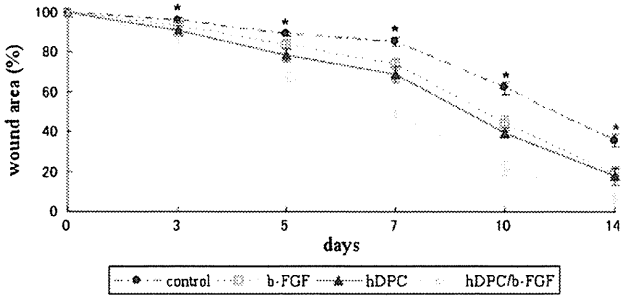

FIGURE 3. Wound area was measured by using Scion Image. The percentage of wound area was calculated as follows: area of actual wound / area of original wound × 100. Analysis of variance, hDPC/b-FGF group versus control group, $*P < 0.05$.

Wound Healing Analysis

Digital photographs were taken at days 0, 3, 5, 7, 10, and 14 to evaluate wound area, which was measured using an image-analyzing software.[18] Wound area was calculated as a percent area of the original wound as follows: area of actual wound / area of original wound × 100.

Histological and Histomorphometric Analysis

Mice were killed at days 7 and 14 after cell transplantation. Skin samples including the wound and 4 mm of the surrounding skin were collected using a scalpel and scissors, fixed in 4% paraformaldehyde and embedded in OCT compound (Tissue-Tek; Miles Inc, Elkhart, IN). Immunofluorescent staining was used to confirm the presence of human type I collagen generated by the injected cells (Rockland Immunochemicals Inc, Gilbertsville, PA). Immunofluorescent staining followed standard methodology. The slides were mounted in the mounting medium with DAPI (Vector Laboratories Inc, Burlingame, CA). And the next slide was stained with hematoxylin and eosin. In addition, histomorphometric analysis used azan staining, following standard methodology. Collagenous fiber area was measured using an image-analyzing software.[18] Collagenous fiber area was calculated as a percent area of dyed light blue. The percentage of collagenous fiber area was calculated as follows: area of dyed light blue / area of all tissue × 100.

Statistical Analysis

Statistical differences among the defect area and collagenous fiber area in each group were evaluated by the Tukey-Kramer test after 1-way analysis of variance. $P < 0.05$ was considered to be statistically significant.

RESULTS

hDPCs/b-FGF Enhance Wound Healing by Macroscopic Findings

Each skin sample was harvested at days 7 and 14. At day 7, all samples were filled with the effusion, and the surface was still raw under macroscopic observation (Fig. 2). On the other hand, at day 14, the wound of hDPC/b-FGF group was almost completely closed in contrast to other groups, and the epithelium appeared thicker (Fig. 2). Digital image analysis showed that the percentage of wound area was 85.38% ± 2.46%, 35.82% ± 3.32% (control group); 74.16% ± 2.78%, 19.30% ± 3.40% (b-FGF group); 69.13% ± 3.96%, 17.83% ± 4.06% (hDPC group); and 48.72% ± 3.22%, 6.50% ± 2.61% (hDPC/b-FGF group) at days 7 and 14, respectively. Both b-FGF group and hDPC group demonstrated accelerated wound healing compared with the control group (Fig. 3). The enhancement appeared at day 5 after implantation and became more evident after day 7. Differences in the mean wound area were statistically significant at all time points after day 7 ($P < 0.05$; Fig. 3). There was no statistically significant difference in wound area observed between hDPC and b-FGF–treated groups at all time points ($P < 0.05$; Fig. 3). The hDPC/b-FGF–treated group appeared to accelerate wound healing compared with the control group (Fig. 3). There was statistically significant difference in wound area observed between the hDPC/b-FGF and control groups at all time points ($P < 0.05$; Fig. 3). The hDPC/b-FGF–treated group accelerated wound healing compared with the b-FGF and hDPC groups (Fig. 3). The enhancement appeared at day 3 after implantation and became more evident after day 5. Differences in the mean wound area were statistically significant at all time points after day 5 ($P < 0.05$; Fig. 3).

Histological Observations

Day 14 after cell transplantation, basophilic nuclei were scattered throughout the tissue, in which great numbers of collagen fibril bundles could be found in the hDPC/b-FGF group by histologic observation (Fig. 4). PKH26 is a lipophilic dye that stains the membrane of viable cells and is distributed among cells when mitosis occurs. It is reported that the fluorescence of PKH26 is not transferred to other cells, but rather to daughter cells with no cellular toxicity. Most of the injected cells labeled with PKH26 were located as a single mass in the subcutaneous tissue in hDPC and hDPC/b-FGF groups (Fig. 4).

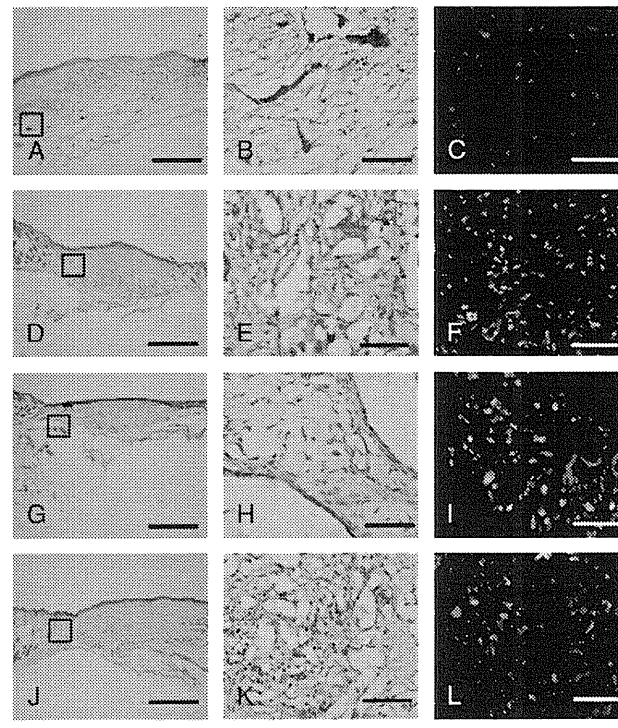

FIGURE 4. Histologic evaluation at day 14 after the procedure. Left and middle panels show hematoxylin and eosin staining, and right panel shows human type collagen staining. Control group is A, B, C; b-FGF group is D, E, F; hDPC group is G, H, I; and hDPC/b-FGF group is J, K, L, respectively. Bar = 3 mm (A, D, G, J); 25 μm (B, C, E, F. H, I, K, L).

© 2011 Mutaz B. Habal, MD

Copyright © 2011 Mutaz B. Habal, MD. Unauthorized reproduction of this article is prohibited.

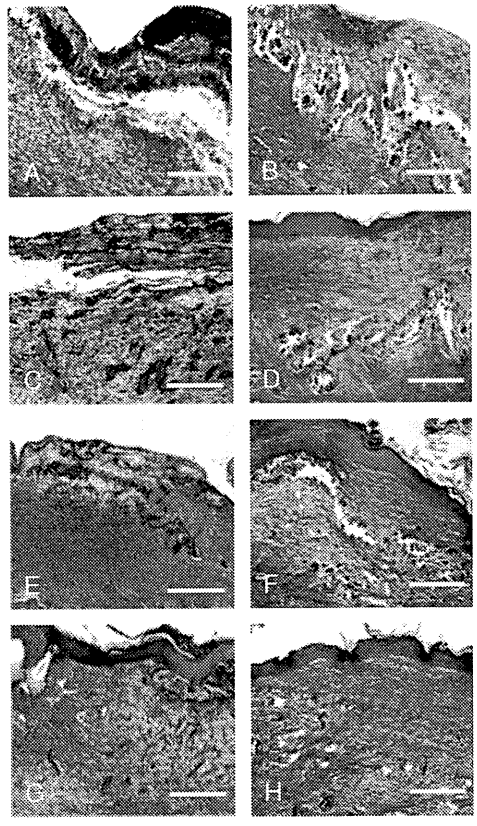

FIGURE 5. Azan staining of the wounds at day 14 after the procedure. Left panel (A, C, E, G) shows day 7, and right panel (B, D, F, H) shows day 14. A and B show results from the control group; C and D show results from the b-FGF group; E and F show results from the hDPC group; G and H show results from the hDPC/b-FGF group, respectively. Bars = 200 μm.

Detection of Human Type I Collagen Produced by Transplanted hDPC and hDPC/b-FGF Groups

Immunohistologic evaluation using anti–human type I collagen antibody was performed to confirm the presence of type I collagen derived from injected hDPC group in mice skin. At day 14, PKH26-positive cells were surrounded by human type I collagen in hDPC and hDPC/b-FGF groups (Fig. 4). These results showed that the hDPC group produced human type I collagen, and bundles of new collagen fibrils were derived from the injected cells.

Histomorphometric Analysis

Wound sections were collected at days 7 and 14 after cell transplantation for azan staining. Images were taken with a conventional microscope with bright field light. At day 7, there appeared to be fewer inflammatory cells in the hDPC/b-FGF group compared with the other groups. All groups were missing epidermis, and the control group was covered with a large amount of clots (Fig. 5). At day 14, many collagen fibrils were observed in the hDPC/b-FGF group compared with the other groups. Collagen fibrils were observed in the hDPC and b-FGF groups compared with the control group (Fig. 5). In addition, epidermis in the hDPC/b-FGF group appeared to be thicker. Reepithelialization was advanced, and the thickening of the epidermis was observed in the hDPC/b-FGF group. The percentages of collagen fibril area at days 7 and 14 were 22.4% ± 2.57%, 28.4% ± 1.74% (control group); 33.4% ± 2.8%, 39% ± 3.03% (b-FGF group); 35.0% ± 4.15%, 40.0% ± 3.03% (hDPC group), and 47.6% ± 3.44%, 52.2% ± 2.99% (hDPC/b-FGF group), respectively (Fig. 6). Significantly increased collagen fibril area in wounded tissue was observed in b-FGF, hDPC, and hDPC/b-FGF groups as compared with the control group at days 7 and 14 ($P < 0.05$; Fig. 6). Moreover, the hDPC/b-FGF group showed significantly higher collagen fibril area compared with the b-FGF and hDPC groups ($P < 0.05$; Fig. 6). There was no statistically significant difference between the b-FGF and hDPC groups ($P < 0.05$; Fig. 6).

DISCUSSION

In this study, we demonstrate for the first time that hDPCs accelerated wound healing, similar to b-FGF, and that they enhanced wound healing more efficiently in the presence of b-FGF. Our immunohistologic staining showed that hDPCs produced human type I collagen, as previously reported, and hDPC/b-FGF group displayed greater production compared with hDPC group. These results meant that b-FGF accelerated human type I collagen production made by hDPCs, the first report of its kind. And our azan staining results demonstrated that collagen fibril production, which meant human collagen made by hDPCs and mice collagen, was consistent to human type I collagen. These results demonstrated that hDPCs enhanced wound healing via increasing collagen production.

There are some kinds of wound healing models. The most simple skin defect model is skin punch-out, but the rodent skin defect is easy to contract and shrink. To eliminate this bias, we used an excisional wound splinting model, resulting in uniform wound closure due to minimization of variations such as skin contraction and wound dressings through granulation and reepithelialization, as reported previously.[19] Therefore, our results are reasonable as a first step to evaluate the wound healing effect of hDPCs. But, rodent and human skin wound healing is considerably different. Researches reported human skin xenografted onto SCID mouse as a chimeric model, which maintains much of its original human skin function.[20] We will use this chimeric model to advance to the next step in our future research.

Of all growth factors, b-FGF is one of the most fascinating in regenerative medicine. Experimental studies have demonstrated that b-FGF administration to the skin wound accelerates angiogenesis, granulation, and epithelialization, resulting in accelerated wound healing.[11] Clinical studies with the use of recombinant b-FGF have shown that it is highly effective and safe for skin ulcers and decubitus ulcer.[21] And b-FGF is also well known as one of the most common

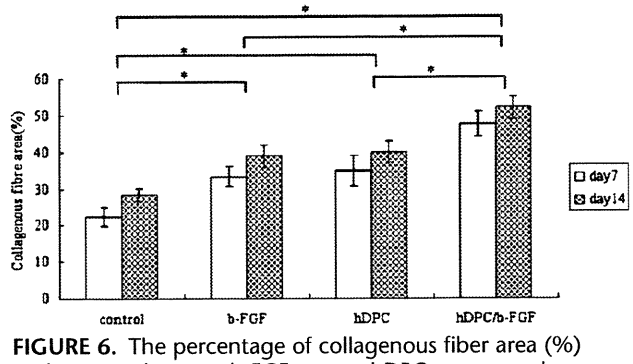

FIGURE 6. The percentage of collagenous fiber area (%) in the control group, b-FGF group, hDPC group, and hDPC/b-FGF group at days 7 and 14 after the procedure. Bar = SD. *$P < 0.05$.

© 2011 Mutaz B. Habal, MD

Copyright © 2011 Mutaz B. Habal, MD. Unauthorized reproduction of this article is prohibited.

reagents to maintain the self-renewal and efficient proliferative capabilities of stem cells.[22] Therefore, we evaluated hDPCs for wound healing with or without b-FGF, and our results showed that b-FGF enhanced human type I collagen production by hDPCs. Our coworkers reported that b-FGF stimulated hDPC proliferation.[23] The fact that hDPC/b-FGF group enhanced collagen production resulted from increasing collagen production per cell and/or hDPC proliferation. Further mechanisms need to be studied for hDPCs with b-FGF in wound healing process.

Stem cells play an important role in regenerative medicine. We can isolate them from born marrow, fat tissue, meniscus, and so on. Dental pulp is a fascinating stem cell source, not only in craniofacial area but also in the whole human body. Compared with other tissue, dental pulp has great advantages; it is "medical waste"—everyone has some dental pulp; there is no need for an invasive, painful procedure; and hDPC has a stem cell population, so it has the capacity to be induced to osteoblasts, chondrocyte, adipocyte, and so on, and express several growth factors such as transforming growth factors β2 and β3 and connective tissue growth factor, nerve growth factor, bone morphogenetic protein 1, and interleukin 1β. It may be suitable for a wide range of human diseases.[10,23] This study demonstrated that hDPCs accelerated wound healing, so it can be an effective, unique stem cell resource for potential of new cell therapies for intractable ulcer such as radiation ulcer, leg ulcer, and decubitus ulcer.

In conclusion, our results showed that hDPCs accelerated wound healing, similar to b-FGF, and they enhanced wound healing more efficiently in the presence of b-FGF. We believe that a better understanding through these investigations will help us understand skin regeneration and the wound healing process and lead us toward developing novel cell therapies for skin defects in the future.

ACKNOWLEDGMENTS

The authors thank M. Okada, A. Yamawaki-Ogata, and A. Kimura for technical assistance, and Drs. H. Hibi and A. Yamamoto for discussion. The authors also thank Kaken Pharmaceutical Co Ltd for the b-FGF.

REFERENCES

1. Boulton AJ, Vileikyte L, Ragnarson-Tennvall G, et al. The global burden of diabetic foot disease. *Lancet* 2005;366:1719–1724
2. Zuk PA, Zhu M, Ashjian P, et al. Human adipose tissue is a source of multipotent stem cells. *Mol Biol Cell* 2002;13:4279–4295
3. Young HE, Steele TA, Bray RA, et al. Human reserve pluripotent mesenchymal stem cells are present in the connective tissues of skeletal muscle and dermis derived from fetal, adult, and geriatric donors. *Anat Rec* 2001;264:51–62
4. Romanov YA, Svintsitskaya VA, Smirnov VN. Searching for alternative sources of postnatal human mesenchymal stem cells: candidate MSC-like cells from umbilical cord. *Stem Cells* 2003;21:105–110
5. Anker In't, Scherjon PS, Kleijburg-van der Keur SA, et al. Isolation of mesenchymal stem cells of fetal or maternal origin from human placenta. *Stem Cells* 2004;22:1338–1345
6. Satoh H, Kishi K, Tanaka T, et al. Transplanted mesenchymal stem cells are effective for skin regeneration in acute cutaneous wounds. *Cell Transplant* 2004;13:405–412
7. Li H, Fu X, Ouyang Y, et al. Adult bone-marrow–derived mesenchymal stem cells contribute to wound healing of skin appendages. *Cell Tissue Res* 2006;326:725–736
8. Kern S, Eichler H, Stoeve J, et al. Comparative analysis of mesenchymal stem cells from bone marrow, umbilical cord blood, or adipose tissue. *Stem Cells* 2006;24:1294–1301
9. Gronthos S, Mankani M, Brahim J, et al. Postnatal human dental pulp stem cells (DPSCs) in vitro and in vivo. *Proc Natl Acad Sci U S A* 2000;97:13625–13630
10. Miura M, Gronthos S, Zhao M, et al. SHED: stem cells from human exfoliated deciduous teeth. *Proc Natl Acad Sci U S A* 2003;100:5807–5812
11. Arthur A, Rychkov G, Shi S, et al. Adult human dental pulp stem cells differentiate toward functionally active neurons under appropriate environmental cues. *Stem Cells* 2008;26:1787–1795
12. Gandia C, Arminan A, Garcia-Verdugo JM, et al. Human dental pulp stem cells improve left ventricular function, induce angiogenesis, and reduce infarct size in rats with acute myocardial infarction. *Stem Cells* 2008;26:638–645
13. Iohara K, Zheng L, Wake H, et al. A novel stem cell source for vasculogenesis in ischemia: subfraction of side population cells from dental pulp. *Stem Cells* 2008;26:2408–2418
14. Gospodarowicz D, Ferrara N, Schweigerer L, et al. Structural characterization and biological functions of fibroblast growth factor. *Endocr Rev* 1987;8:95–114
15. Burgess WH, Maciag T. The heparin-binding (fibroblast) growth factor family of proteins. *Annu Rev Biochem* 1989;58:575–606
16. Rifkin DB, Moscatelli D. Recent developments in the cell biology of basic fibroblast growth factor. *J Cell Biol* 1989;109:1–6
17. Schweigerer L. Basic fibroblast growth factor as a wound healing hormone. *Trends Pharmacol Sci* 1988;9:427–428
18. *Scion Image* [computer program]. *Version 0.4.0.3*. Frederick, MD: Scion Corporation; 2001
19. Galiano RD, Michaels J, Dobryansky M, et al. Quantitative and reproducible murine model of excisional wound healing. *Wound Repair Regen* 2004;12:485–492
20. Boehncke WH, Kaufmann R. Human to mouse xenotransplantation models complement transgenic and know-out mice [Comment on the contribution by K. Sellheyser: transgenic mice as models for skin diseases]. *Hautarzt* 1996;47:475–476
21. Ishibashi Y, Harada S, Takemura T, et al. Clinical effectiveness of KCB-1(bFGF) on patients with skin ulcerations clinical trial for 12 weeks [in Japanese]. *J Clin Ther Med* 1996;12:2117–2129
22. Ng F, Boucher S, Koh S, et al. PDGF, TGF-beta, and FGF signaling is important for differentiation and growth of mesenchymal stem cells (MSCs): transcriptional profiling can identify markers and signaling pathways important in differentiation of MSCs into adipogenic, chondrogenic, and osteogenic lineages. *Blood* 2008;112:295–307
23. Nakamura S, Yamada Y, Katagiri W, et al. Stem cell proliferation pathways comparison between human exfoliated deciduous teeth and dental pulp stem cells by gene expression profile from promising dental pulp. *J Endod* 2009;35:1536–1542

© 2011 Mutaz B. Habal, MD

Copyright © 2011 Mutaz B. Habal, MD. Unauthorized reproduction of this article is prohibited.

Annals of Biomedical Engineering, Vol. 39, No. 7, July 2011 *(© 2011)* pp. 1872–1881
DOI: 10.1007/s10439-011-0327-0

Osteogenic Induction of Bone Marrow-Derived Stromal Cells on Simvastatin-Releasing, Biodegradable, Nano- to Microscale Fiber Scaffolds

RYU WADAGAKI,[1] DAIKI MIZUNO,[1,4] AIKA YAMAWAKI-OGATA,[2] MAKOTO SATAKE,[3] HIROAKI KANEKO,[3] SUMITAKA HAGIWARA,[1] NORIYUKI YAMAMOTO,[1] YUJI NARITA,[2] HIDEHARU HIBI,[1] and MINORU UEDA[1]

[1]Department of Oral and Maxillofacial Surgery, Nagoya University Graduate School of Medicine, Nagoya 466-8550, Japan; [2]Department of Cardiac Surgery, Nagoya University Graduate School of Medicine, Nagoya 466-8550, Japan; [3]Integrative Technology Research Institute, New Business Development Group, Teijin Limited, Tokyo 191-8512, Japan; and [4]Oral and Maxillofacial Surgery, Chubu Rosai Hospital, Nagoya 455-8530, Japan

(Received 28 October 2010; accepted 23 February 2011; published online 18 May 2011)

Associate Editor Smadar Cohen oversaw the review of this article.

Abstract—Tissue engineering is an effective approach for the treatment of bone defects. Statins have been demonstrated to promote osteoblastic differentiation of bone marrow-derived stromal cells (BMSCs). Electrospun biodegradable fibers have also shown applicability to drug delivery in the form of bone tissue engineered scaffolds with nano- to microscale topography and high porosity similar to the natural extracellular matrix (ECM). The aim of this study was to investigate the feasibility of a simvastatin-releasing, biodegradable, nano- to microscale fiber scaffold (SRBFS) for bone tissue engineering with BMSCs. Simvastatin was released from SRBFS slowly. BMSCs were observed to spread actively and rigidly adhere to SRBFS. BMSCs on SRBFS showed an increase in alkaline phosphatase activity 2 weeks after cell culture. Furthermore, osteoclastogenesis was suppressed by SRBFS *in vitro*. The new bone formation and mineralization in the SRBFS group were significantly better than in the biodegradable fiber scaffold (BFS) without simvastatin 12 weeks after implantation of the cell-scaffold construct into an ectopic site on the murine back. These results suggest that SRBFS promoted osteoblastic differentiation of BMSCs *in vitro* and *in vivo*, and demonstrate feasibility as a bone engineering scaffold.

Keywords—Bone tissue engineering, Statin, Osteogenic differentiation, Electrospun biodegradable fiber scaffold, BMSCs.

INTRODUCTION

For reconstruction of a bone defect, the efficacy of various tissue engineering approaches using many kinds of scaffolds, bioactive substances, and cells has been demonstrated.[2,4] Although various cell sources have been introduced for application to bone tissue engineering, these cells commonly have been required for osteoinductive steps in the cell culture process before transplantation. For example, bone morphogenetic proteins (BMPs) are probably the most important osteoinductive factor in bone metabolism.[15] However, for broader clinical application, recombinant BMPs still pose problems in terms of safety and cost.[8,20]

For these reasons, this study focused on "statins" as osteoinductive factors that have been widely and safely used for the treatment of hyperlipidemia for more than two decades. Some studies have reported anabolic effects of statins on bone formation.[11] Also, statins are small, stable molecules that are not susceptible to proteolytic degradation and are stably produced, making them more cost effective than recombinant BMPs to produce.[11] Statins reportedly promoted osteogenic differentiation of bone marrow-derived stromal cells (BMSCs) and stimulated expression of BMP-2,[22] but suppressed osteoclastogenesis through blocking of the RANKL-induced NF-κB activation pathway.[2]

Meanwhile, our previous studies reported a sustained drug delivery system (DDS) using electrospinning biodegradable fiber with various types of drugs.[12,13,31] Sustained drug release can be adjusted by

Address correspondence to Yuji Narita, Department of Cardiac Surgery, Nagoya University Graduate School of Medicine, Nagoya 466-8550, Japan. Electronic mail: gakiryu@med.nagoya-u.ac.jp, ynarita@med.nagoya-u.ac.jp

0090-6964/11/0700-1872/0 © 2011 Biomedical Engineering Society

modification in the polymer degradation and can contribute to minimizing systemic influences and adverse side effects, while maximizing the local effects. Furthermore, the electrospinning process provides engineering scaffolds with nano- to microscale topography and high porosity similar to the natural extracellular matrix (ECM).[21] The large area-to-volume ratio of the fibers combined with their porous structure are beneficial for cell adhesion, proliferation,[27] migration,[32] and differentiation.[3] The high porosity of nano- to microscale fiber scaffolds assures more structural space for cell adaptation and promotes efficient exchange of nutrient and metabolic waste.

Therefore, we hypothesized that statin with electrospun biodegradable nano- to microscale fiber is a satisfactory combination for bone tissue engineering scaffold. A simvastatin-releasing, biodegradable, nano- to microscale fiber scaffold (SRBFS) was fabricated using a biodegradable polymer with simvastatin as the osteoinductive factor by an electrospinning procedure. The current study characterizes the complexes of SRBFS and BMSCs which have been major cell sources for bone regeneration, *in vitro* and *in vivo*, using an ectopic bone formation model in mice.

MATERIALS AND METHODS

Animals

All animal experiments were performed in accordance with the "Guidelines and Regulations for Use and Care of Animals in Nagoya University" and approved by the "Animal Experiment Advisory Committee of the Nagoya University School of Medicine." This study used mice (C57/BL/6J, 4 weeks old, male) purchased from the Chubu Kagaku Shizai Corporation (Nagoya, Japan).

Isolation and Expansion of BMSCs

Mouse BMSCs were obtained by established techniques.[10] BMSCs were seeded in a culture medium containing α-MEM (Invitrogen, Carlsbad, CA, USA) supplemented with 10% fetal bovine serum (FBS) and 1% penicillin/streptomycin, and were subcultured by 4–6 passages and used for experiments. Osteogenic factors were not added in the culture medium. Characterization of BMSCs was determined by flow cytometry. Cells were labeled with the antibodies CD11b and Sca-1 (eBioscience, CA, USA). Cells used for this study were more than 70% positive for Sca-1 and less than 10% positive for CD11b (data not shown).

Fabrication of Simvastatin-Releasing, Biodegradable, Nano- to Microscale Fiber Scaffold (SRBFS)

SRBFS and BFS fabrication methods were the same as previously described.[12] In brief, simvastatin (Toronto Research Chemicals, Inc., North York, ON, Canada) (MW = 418.57) was mixed with biodegradable polymer to fabricate SRBFS, and not mixed to fabricate BFS. Poly(L-lactide-*co*-glycolide) (IV = 1.15 dL/g), which consists of 50% of each polymer, was prepared for the biodegradable polymer. To fabricate the nano- to microscale fiber, an electrospinning procedure was used. The polymer solution was added using a 1-mL syringe with a right angle-shaped metal capillary attached to it. The circular orifice of the capillary had an inner diameter of 1.2 mm. A flat counter electrode was located 35 cm from the capillary tip. Pressure was applied to the solution in the syringe, gradually forcing the piston to maintain a steady flow of solution from the capillary outlet. The flow rate of the polymer solution was 0.3 mL/min. The applied voltage ranged from 10 to 15 kV. The fibers released in the atmosphere were electrostatically removed and trapped with a rod-shaped collector located 20 cm from the capillary tip. The SRBFS shows a "cotton wool"-like formation (Fig. 1a). The fibers ranged from 500 nm to 10 μm in diameter (Figs. 1c, 1d). This configuration is flexible, making it easy to handle any bone defect. The simvastatin content in the SRBFS was 0.025 wt%.

Test of Simvastatin Release from SRBFS

The release test was carried out according to a previous report.[26] Five mg of SRBFS was placed in 1 mL phosphate-buffered saline (PBS) at 37 °C, and the PBS was exchanged at 1, 2, 3, 5, 7, 14, and 28 days, respectively. The PBS supernatant was freeze-dried, and dissolved in 1,1,1,3,3,3-hexafluoro-2-propanol (HFP) (Wako, Osaka, Japan). After centrifugation (8000 rpm, 5 min, 4 °C), the supernatant absorbance was measured at a wavelength of 248 nm while the simvastatin concentration was determined from the standard curve prepared with the HFP containing various amounts of simvastatin.

Cell Seeding on Scaffold

Sterilized scaffolds (0.2 cm^3 in volume, 5 mg in mass) were incubated in the culture medium for 12 h prior to cell seeding in a 96-well plate. Approximately 5×10^5 cells were suspended in 30 μL of culture medium and slowly injected into and around the nanofibrous scaffolds in a 96-well plate. Cell-scaffold constructs were subsequently cultured in α-MEM (Invitrogen, Carlsbad, CA, USA) supplemented with

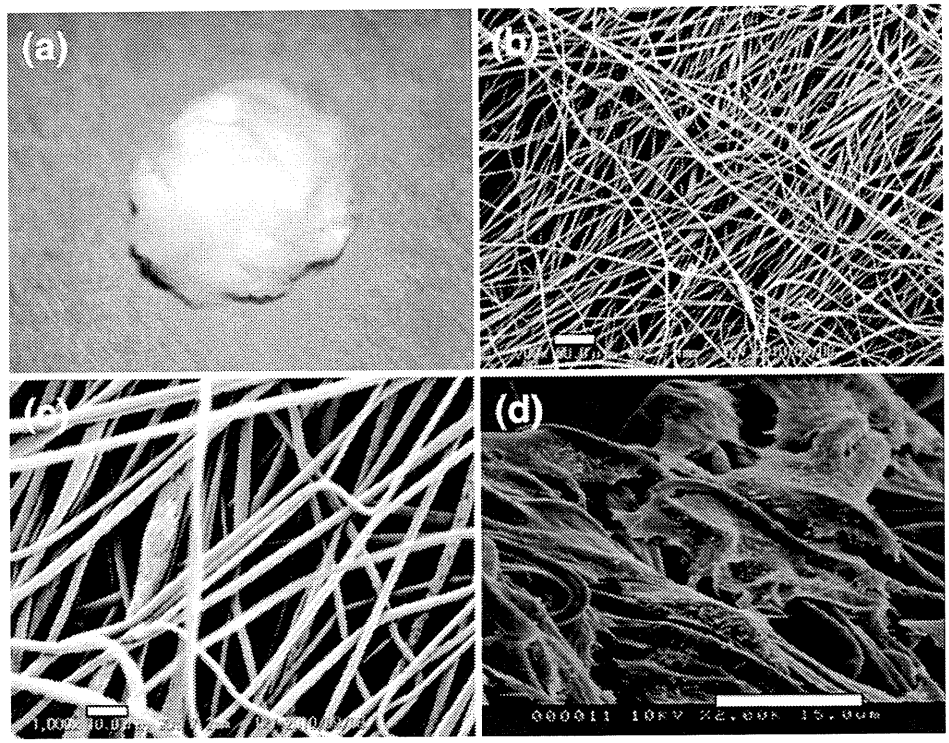

FIGURE 1. (a) Overall appearance of SRBFS. SRBFS appears to have a "cotton wool"-like formation. (b) SEM (original magnification, ×200) of SRBFS reveals a non-woven fabric appearance. Scale bar: 50 μm. (c) SEM (original magnification, ×1000) of SRBFS showed that the polymer fiber was 500 μm-10 nm in diameter. Scale bar: 10 μm. (d) FESEM image of BMSCs seeded on SRBFS after 7 days. Scale bar: 15 μm.

10% FBS and 1% penicillin/streptomycin for 7 or 14 days in a humidified environment with 5% CO_2 at 37 °C before *in vitro* assays and cultured for 14 days before *in vivo* assays, with the medium changed every 3 days. Osteogenic factors, such as dexamethasone and BMP-2, were not added in the culture medium during the culture period.

Scanning Electron Microscopic Study

BMSCs cultured on SRBFS for 7 days were washed with PBS to remove non-adherent cells, fixed in 2.5% glutaraldehyde, and then post-fixed in 4% osmium tetroxide. The samples were dehydrated through a series of graded alcohol solutions. After *t*-butyl-alcohol freeze-drying, cellular constructs were sputter-coated with osmium and observed under field emission scanning electron microscopy (FESEM) (S-800, Hitachi, Tokyo, Japan) at 10 kV.

Measurement of Alkaline Phosphatase Activity

Seven and 14 days after seeding on BFS and SRBFS, BMSCs were assayed for alkaline phosphatase (ALP) activity. ALP activity was measured with a commercial *p*-nitrophenyl phosphate tablet set (Sigma Chemical, St. Louis, MO, USA) and a cell counting kit (WST-8: Dojindo, Kumamoto, Japan). Cell numbers were analyzed according to the manufacturer's protocol. Briefly, 100 μL of reagents was added to each well containing 1 mL of fresh medium with cell-scaffold constructs, incubated for 3 h, and absorbance measured on a spectrophotofluorometer (Bio-Rad Laboratories, Hercules, CA, USA). Cell numbers were determined from the standard calibration curve by measuring the absorbance. After WST-8 analysis, each well and scaffolds were washed three times with PBS, and 800 mL of *p*-nitrophenyl phosphate solution was added to each well. After 10 min of incubation at 37 °C, the reaction was stopped with 800 mL of 3 N NaOH and the absorbance of *p*-nitrophenol was measured. ALP activities were normalized to the number of cells calculated according to the WST-8 assay.

In Vitro Osteoclast Formation

Mouse osteoclasts were prepared from bone marrow cells as previously described.[25] Briefly, bone marrow cells were obtained by flushing the femurs and tibiae of mice and cultured in α-MEM containing 10% FBS for 1 day. Non-adherent cells were harvested and cultured in α-MEM (5×10^4 cells per well in a 24-well

plate) with 10% FBS containing 10 ng/mL M-CSF (R&D Systems, Inc., Minneapolis, MN, USA). Two days later, adherent cells were used as bone marrow-derived monocyte/macrophage precursor cells (BMMs) after washing out the non-adherent cells. These cells were cultured with 100 ng/mL RANKL (R&D Systems, Inc., Minneapolis, MN, USA) and 10 ng/mL M-CSF (R&D Systems), and co-cultured with 5 mg of SRBFS or BFS. Indirect co-culture systems for BMMs and SRBFS or BFS were established using a 24-well plate with 0.4-μm pore, 10-μm thickness polyester membrane cell culture inserts (Corning, NY, USA). BMMs were cultured on the plate well, and SRBFS or BFS were then placed in the insert. After 5 days, cultured cells were fixed and stained for tartrate-resistance acid phosphatase (TRAP) (Wako Pure Chemical Industries, Osaka, Japan). TRAP-positive multinucleated cells with greater than three nuclei were counted as osteoclasts.

Cell-Scaffold Construct Implantation

After the mice were anesthetized by diethyl ether inhalation (Sigma-Aldrich, Tokyo, Japan), small incisions were made on the bilateral dorsal skin. A cell-seeded SRBFS was immediately implanted into the left subcutaneous pocket on the murine back, a cell-seeded BFS into the right, and the skin was then closed with sutures.

Radiographic Analysis

Twelve weeks after transplantation, the samples were assessed by X-ray (G1 meisterII FLUOREX, Toshiba, Tokyo, Japan), and the conditions used were 40 kV and 200 mA for 0.640 s. Under these defined conditions, exposures were carried out with an aluminum wedge that allowed the radiographic densities to be computed later. The radiographic density of the harvested transplant area was estimated as aluminum thickness by measuring with image analysis software (Image J, Scion Corporation, Frederick, MD, USA).

Histological Analysis of Ectopic Bone Formation In Vivo

Six and 12 weeks after transplantation, the implants were harvested for analysis, immediately fixed in 4% (w/v) paraformaldehyde and decalcified with a commercially available decalcifying solution (K-CX, Falma Corporation, Tokyo, Japan) for about 2 days before embedding in paraffin. Three-micrometer serial sections were cut and processed for routine histological observation by staining with hematoxylin and eosin (H–E) and for immunochemistry. The bone formation area was measured using image analysis software (Image J, Scion Corporation, Frederick, MD, USA), and then expressed as the percentage of bone area in the total cross-sectional area. Immunohistochemical analysis was performed using bone sialoprotein (BSP) polyclonal antibody (1:200) (LSL Co., Cosmo Bio, Tokyo, Japan) as primary antibody. A biotinylated secondary antibody (1:200) (rabbit anti-mouse IgG) (Vector Laboratories, CA, USA) was applied, and an avidin–biotin complex using Vectastain ABC kit (Vector Laboratories). Finally, slides were reacted with 0.1% w/v 3,3′-diaminobenzidine tetrahydrochloride solution and counterstained with hematoxylin solution. The BSP-positive cells were counted as follows. At least 10 fields for each section were randomly captured (×200 magnification, 5 samples in total), and then all cells and BSP depositing cells in the fields were counted. The ratio of BSP-positive cells was calculated as the percentage of BSP-positive cells in all cells.

Mineralization Analysis

Bone mineralization was analyzed by determining the amount of deposited calcium using a method reported previously.[14] Twelve weeks after transplantation, retrieved implant samples were rinsed with PBS and homogenized with 0.6 N HCl, and calcium was then extracted by shaking them for 4 h at 4 °C. The lysate was then centrifuged at 1,000×g for 5 min, and the supernatant was used to quantify calcium content in samples by spectrophotometry using a Calcium Colorimetric Assay Kit (BioVision, Mountain View, CA, USA). Five minutes after the addition of reagents, the absorbance of the samples was read at 575 nm using a microplate reader (SmartSpeckTM3000, Bio-Rad, Tokyo, Japan). Calcium content was calculated from a standard curve generated from the serial dilution of a calcium standard solution (BioVision).

Statistical Analysis

Statistical significance was analyzed either by one-way factorial analysis of variance (ANOVA) or unpaired t test. A p value less than 0.05 was considered statistically significant. Quantitative data were statistically analyzed to express the mean ± the standard deviation.

RESULTS

Morphology of BMSCs on SRBFS

The FESEM image of BMSCs cultured on SRBFS for 7 days shows that the cells spread actively, rigidly

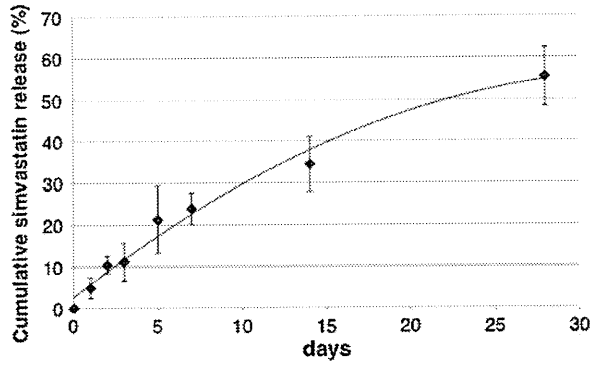

FIGURE 2. Cumulative release of SRBFS *in vitro*. The curve is intended to lead the eye. Values represent the mean ± standard deviation (n = 3).

adhered to the fibers, and ECM production by cells was then observed (Fig. 1d).

In Vitro Simvastatin Release from SRBFS

The *in vitro* release pattern of simvastatin from SRBFS is shown in Fig. 2. On day 1, approximately 5% of the simvastatin was released from SRBFS. Thereafter, simvastatin release was slow and at a constant rate until day 7. By day 14, about 35% of the loaded simvastatin was released, and about 55% of it from SRBFS by day 28.

Effect of Released Simvastatin on BMSC Osteogenic Differentiation

To examine whether released simvastatin had an effect on osteogenic differentiation of BMSCs, ALP activity was measured *in vitro* on days 7 and 14 (Fig. 3). Although there was no significant difference between the SRBFS and BFS groups on day 7, the ALP activity of the SRBFS groups was significantly higher than that of the BFS groups ($p < 0.05$) on day 14.

Effect of Released Simvastatin on Inhibition of Osteoclastogenesis

The effect of simvastatin released from SRBFS on osteoclastogenesis was examined. Figures 4a and 4b revealed that BMMs incubated with BFS differentiated into many osteoclasts, whereas BMMs incubated with SRBFS differentiated into only a few osteoclasts. As shown in Fig. 4c, the total number of TRAP-positive multinucleated osteoclasts in the SRBFS group was significantly inhibited compared with the BFS group.

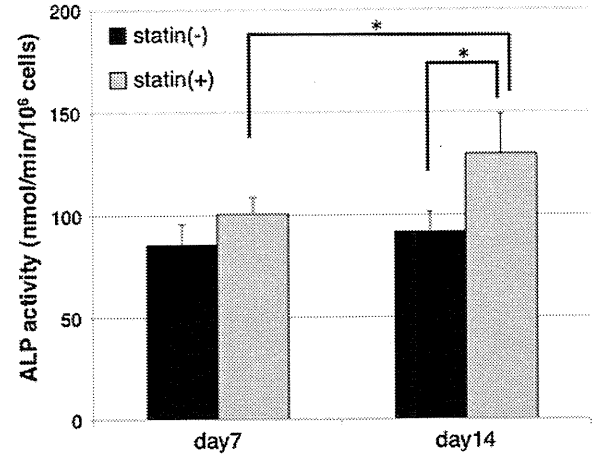

FIGURE 3. ALP activity of BMSCs on SRBFS and BFS measured on days 7 and 14. Values represent the mean ± standard deviation (n = 5). Statistically significant difference is labeled (*$p < 0.05$).

Radiographic Analysis

Figure 5a shows X-ray photographs 12 weeks after transplantation. Round-shaped radiopaque tissues were found on both sides. Statistical analysis showed that SRBFS radiodensity was significantly higher than in the BFS group 12 weeks after transplantation (Fig. 5b).

Histological and Immunohistochemical Analysis

Figures 6a–6d show H–E staining sections 6 and 12 weeks after transplantation. Six weeks after transplantation, an extensive immature mineral formation had been observed in both groups (Figs. 6a, 6b). At 12 weeks, mainly woven bone and focal trabecular bone with a lamellar appearance were observed. Numerous osteoblasts lining the woven bone and mineral formation indicated active bone formation (Figs. 6c, 6d). Immunohistochemical staining with BSP was performed using the section harvested from implants taken from mice (Figs. 6e, 6f). BSP was positive in a wide range of intracellular and extracellular tissue regardless of statin content. Newly formed bone area and the ratio of BSP-positive cells in the SRBFS groups were significantly higher than those in the BFS groups 12 weeks after implantation (Figs. 7a, 7b).

Mineralization Analysis

To determine the mineralized matrix deposition in the generated tissue, calcium deposition was measured. Calcium deposition in the SRBFS group was higher than in the BFS group (Fig. 7c).

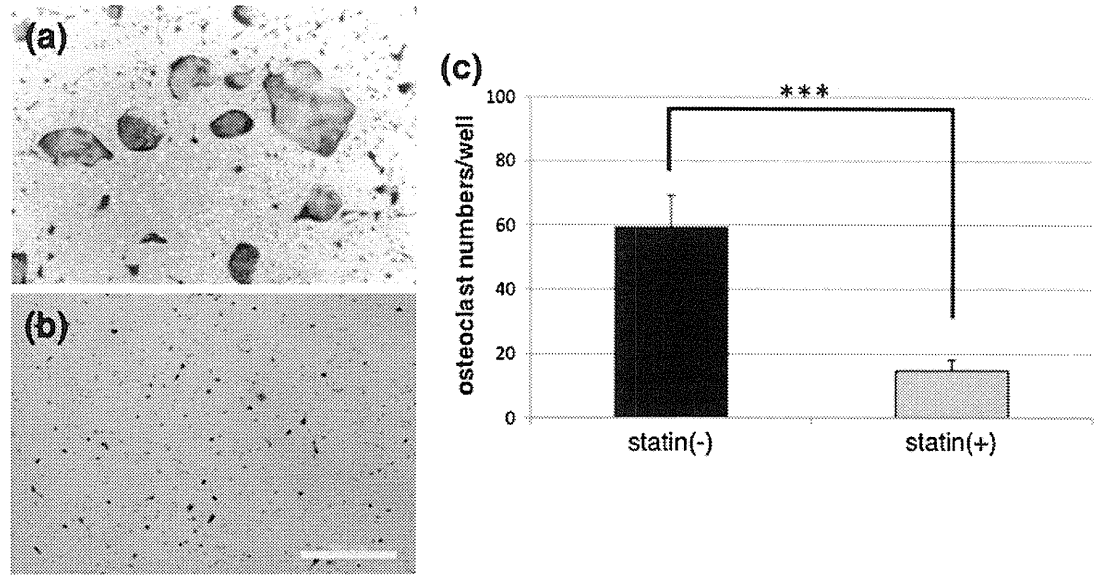

FIGURE 4. Simvastatin released from SRBFS inhibits RANKL-induced osteoclastogenesis 5 days after stimulation. Cells were cultured for 5 days with (a) SRBFS and (b) BFS after RANKL treatment and stained for TRAP expression. Scale bar: 500 μm. (c) The total number of TRAP-positive multinucleated osteoclasts (i.e., those containing three nuclei) per well were counted. Values represent the mean ± standard deviation (n = 5). Statistically significant difference is labeled (*$p < 0.001$).**

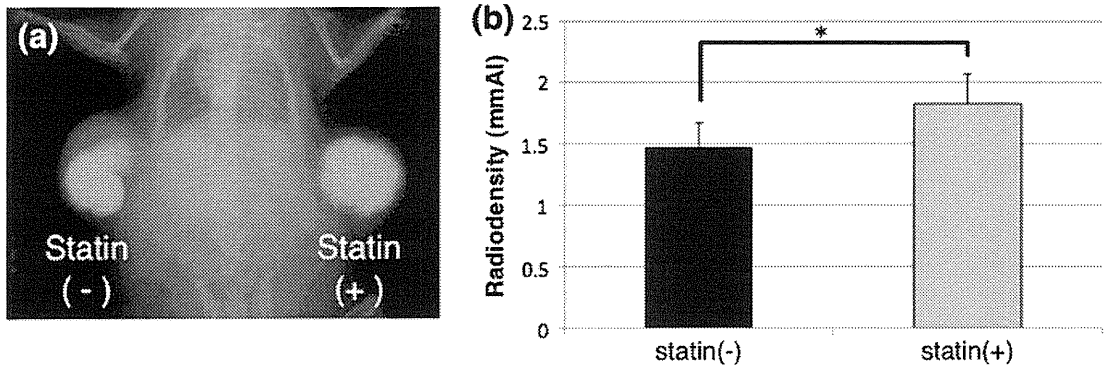

FIGURE 5. (a) X-ray photograph of ectopically formed bone 12 weeks after transplantation. (b) Radiographic density in the transplants 12 weeks after transplantation (n = 4). Values represent the mean ± standard deviation. Statistically significant difference is labeled (*$p < 0.05$).

DISCUSSION

Our current study is the first report to describe the ectopic bone formation of mice using the complex of statin-releasing biodegradable nano- to microscaled fiber scaffolds and BMSCs, and our scaffold is applicable for bone tissue engineering.

Our *in vitro* studies revealed that the effects of simvastatin released from SRBFS on osteoblastogenesis and osteoclastogenesis were effective for osteogenesis. ALP activity of BMSCs seeded on the SRBFS for 2 weeks was significantly elevated, and the number of osteoclasts differentiated from precursor cells was significantly decreased in the SRBFS. Thus, we demonstrated that simvastatin released from SRBFS promotes simultaneously osteoblastic differentiation of BMSCs and inhibits osteoclastogenesis of BMMs. However, in this study, the inhibition of osteoclastogenesis was demonstrated only *in vitro*, and further *in vivo* assays are needed to evaluate in more detail the effect of simvastatin on osteoclastogenesis.

In several previous studies, the simvastatin was loaded in various materials for bone tissue engineering, such as gelatin hydrogel,[26] α-tricalcium phosphate,[17] methylcellulose gel,[23] collagen sponge,[28] and calcium sulfate.[18] Most of these studies reported positive effects for bone regeneration. In this study, the statin-loaded biodegradable fiber from the electrospinning procedure was developed to release the simvastatin gradually over

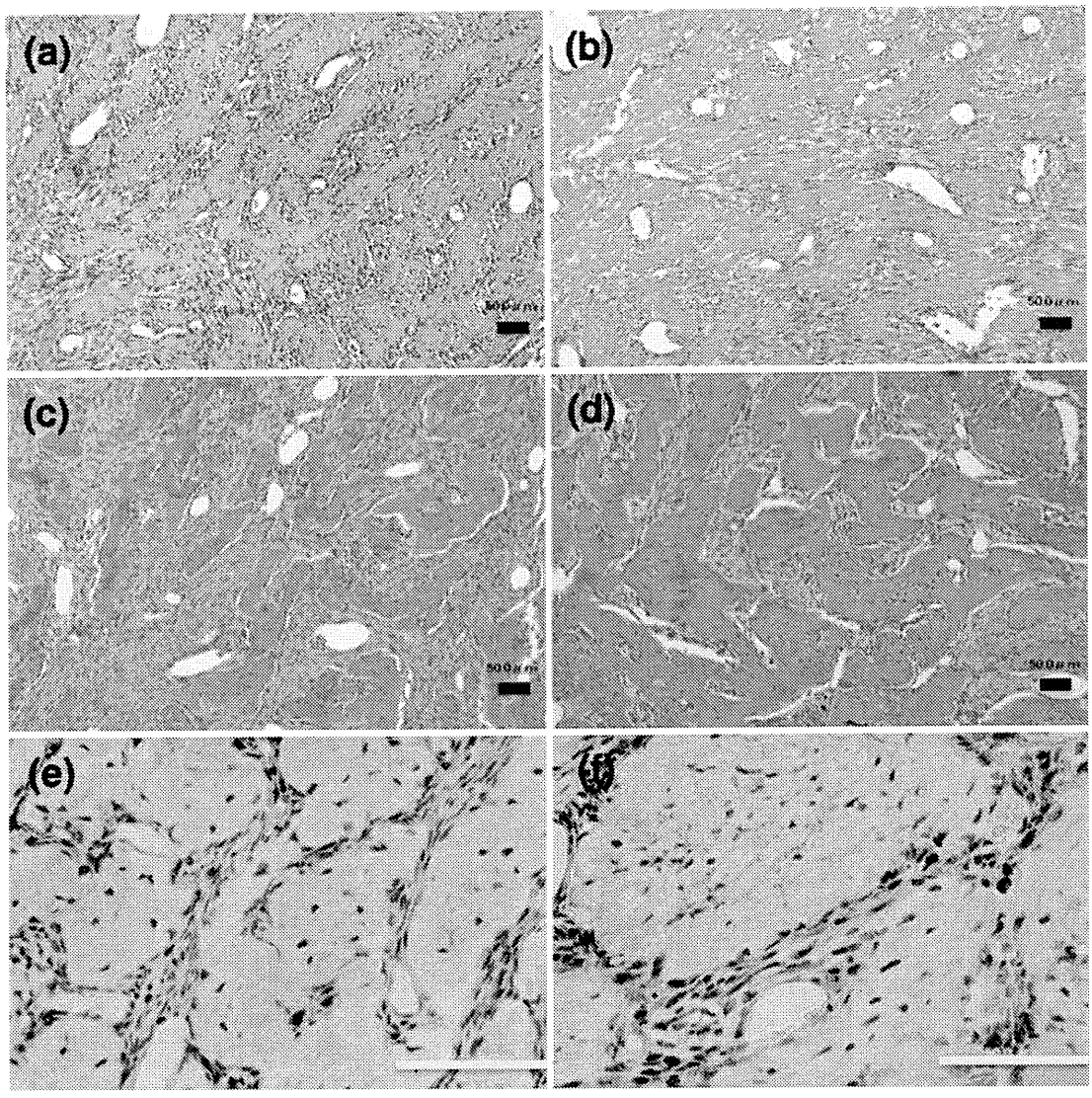

FIGURE 6. Histological and immunohistochemical analyses 6 and 12 weeks after implantation. (a–d) H–E staining, (a, b) at 6 and (c, d) 12 weeks, while (e, f) show immunohistochemical staining with BSP at 12 weeks. (a, c, e): BFS (b, d, f): SRBFS. Scale bar: 50 μm.

time. The mechanism of sustained release of simvastatin takes place through degradation of biodegradable polymer by hydrolysis. The electrospinning procedure makes it possible to control the release of a wide range of antibiotics[5] and anticancer drugs[30] to proteins[9,16] and DNA[16] for application in tissue engineering. However, this technique has a limitation in that some organic solvents used to prepare the polymer solutions may also degrade the drugs.[1]

To optimize this simvastatin-releasing system, we determined the simvastatin content of SRBFS on the basis of the simvastatin release test of SRBFS and preliminary studies. BMSCs were cultured in various concentrations (0.5–5.0 μM) of simvastatin, and cell proliferation and ALP activity were then evaluated. These preliminary studies suggested that the appropriate concentration of simvastatin was 0.5–1 μM in *in vitro* culture with respect to cell proliferation (cytotoxicity) and ALP activity (data not shown). BMSCs could not proliferate in a medium containing more than 2.5 μM of simvastatin. Though the apoptotic effect of high-dose simvastatin has been reported in several studies,[6,7] more than a certain concentration of simvastatin is apparently needed for osteogenic induction and osteoclastogenesis inhibition. However, it is difficult to measure exactly a local simvastatin-exposed dose to cells with such direct adhesion to fiber as in this study. Besides the simvastatin content of the biodegradable polymer, the dose of simvastatin released from fibers is also dependent on the composition

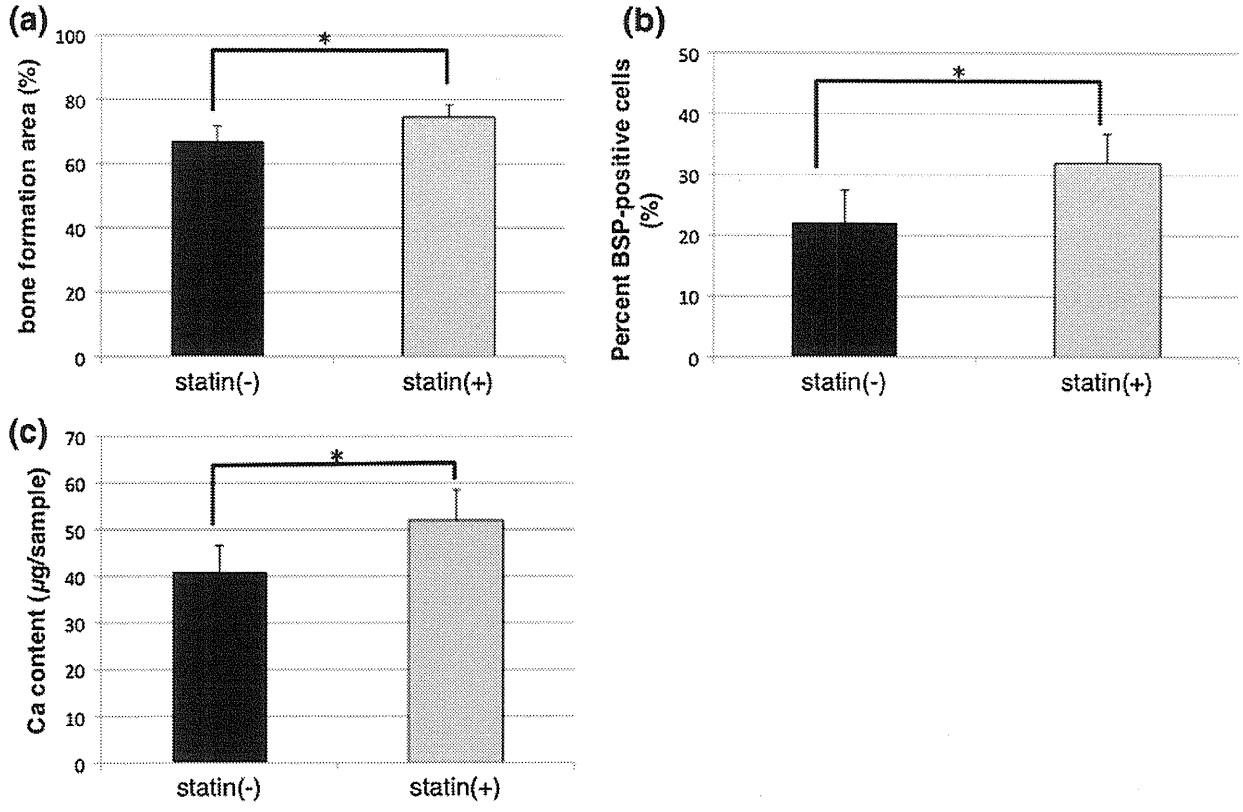

FIGURE 7. (a) Bone formation area analyzed by H&E staining 12 weeks after implantation (n = 5). (b) Percent BSP-positive cells as determined by immunohistochemical staining with BSP 12 weeks after implantation (n = 5). (c) Accumulated calcium content per sample 12 weeks after implantation (n = 4). Values represent the mean ± standard deviation. Statistically significant difference is labeled (*$p < 0.05$).

of the polymer (polyglycolic acid (PGA), polylactic acid (PLA), polycaplolacton (PCL), and their co-polymers), along with the rate of copolymerization, and fiber diameter. These factors need to be taken into consideration for optimization of drug release in the future. If the local dose of statin released from the scaffold can be regulated appropriately, this strategy could not only minimize damage to cells at high concentrations, but also reduce the drug dosage needed, and thereby be more effective, safe and inexpensive for bone tissue engineering.

Histological examination 12 weeks after transplantation revealed that the amount of new bone formation in the SRBFS group was significantly higher than in the BFS group. Twelve weeks after transplantation, SRBFS alone without BMSCs did not induce bone formation in the murine back (data not shown). These data suggest that BMSCs could play an important role in ectopic bone formation, and statin may promote the osteogenic activity of BMSCs for bone formation. To the best of our knowledge, successful ectopic bone formation *in vivo* using statin-releasing materials without cell transplantation has not been reported in detail. A previous study reported that statin-loaded biodegradable fiber without seeding cells was applied for healing a critical-size bone defect of an animal,[19] and suggested the necessity of cell-seeded scaffolds. While statin alone was insufficient to induce ectopic bone formation, in combination with preosteogenic cells statin resulted in significant promotion of such formation.

Analyses of radiodensity and calcium deposition were performed to determine the mineralized matrix deposition in scaffolds. Some studies reported that local application of statin could increase bone mineral density.[17,29] Our results reveal that the SRBFS group showed significantly higher mineralization, which suggests that statin may play a pivotal role in mineralization during bone maturation. The osteogenic phenotype of BMSCs seeded onto SRBFS was also assessed by the immunodetection of a specific osteoblastic protein, BSP. High BSP expression confirms the presence of mature osteoblasts.[4] These results suggest that released simvastatin may also promote bone maturation as well as osteogenic induction.

Our results demonstrate that the combination of BMSCs and biodegradable fiber scaffolds releasing simvastatin, which acts like an osteoinductive factor,

may be an excellent strategy for bone tissue engineering applications. We here combined simvastatin-releasing materials with cell transplantation to a bone tissue engineering scaffold in an attempt to form new ectopic bone. This "cotton wool"-like configuration fiber scaffold can flexibly fit any shape of a local bone defect site. Furthermore, the present result of ectopic bone formation *in vivo* shows that this strategy has potential for application to large bone defects under severe conditions. Although its clinical utility for large bone defects is limited by its relatively poor mechanical properties, these can be improved by combination with other materials.

In summary, our data suggest that sustained simvastatin release from biodegradable nano-microfiber scaffolds promotes osteogenic differentiation of BMSCs and enhances new bone formation *in vivo*.

ACKNOWLEDGMENTS

This work was supported by a grant-in-aid for "Young Scientists (start up)" (20890100) from the Ministry of Education, Culture, Sports, Science, and Technology of Japan, and by a grant for "COE for Education and Research of Micro-Nano Mechatronics Nagoya University Global COE Program."

REFERENCES

[1]Ahmad, Z., H. B. Zhang, U. Farook, M. Edirisinghe, E. Stride, and P. Colombo. Generation of multilayered structures for biomedical applications using a novel tri-needle coaxial device and electrohydrodynamic flow. *J. R. Soc. Interface* 5:1255–1261, 2008.

[2]Ahn, K. S., G. Sethi, M. M. Chaturvedi, and B. B. Aggarwal. Simvastatin, 3-hydroxy-3-methylglutaryl coenzyme A reductase inhibitor, suppresses osteoclastogenesis induced by receptor activator of nuclear factor-kappaB ligand through modulation of NF-kappaB pathway. *Int. J. Cancer* 123:1733–1740, 2008.

[3]Badami, A. S., M. R. Kreke, M. S. Thompson, J. S. Riffle, and A. S. Goldstein. Effect of fiber diameter on spreading, proliferation, and differentiation of osteoblastic cells on electrospun poly(lactic acid) substrates. *Biomaterials* 27:596–606, 2006.

[4]Bianco, P., M. Riminucci, E. Bonucci, J. D. Termine, and P. G. Robey. Bone sialoprotein (BSP) secretion and osteoblast differentiation: relationship to bromodeoxyuridine incorporation, alkaline phosphatase, and matrix deposition. *J. Histochem. Cytochem.* 41:183–191, 1993.

[5]Bolgen, N., I. Vargel, P. Korkusuz, Y. Z. Menceloglu, and E. Piskin. In vivo performance of antibiotic embedded electrospun PCL membranes for prevention of abdominal adhesions. *J. Biomed. Mater. Res. B Appl. Biomater.* 81:530–543, 2007.

[6]Fromigue, O., E. Hay, D. Modrowski, S. Bouvet, A. Jacquel, P. Auberger, and P. J. Marie. RhoA GTPase inactivation by statins induces osteosarcoma cell apoptosis by inhibiting p42/p44-MAPKs-Bcl-2 signaling independently of BMP-2 and cell differentiation. *Cell Death Differ.* 13:1845–1856, 2006.

[7]Garcia-Roman, N., A. M. Alvarez, M. J. Toro, A. Montes, and M. J. Lorenzo. Lovastatin induces apoptosis of spontaneously immortalized rat brain neuroblasts: involvement of nonsterol isoprenoid biosynthesis inhibition. *Mol. Cell. Neurosci.* 17:329–341, 2001.

[8]Hwang, C. J., A. R. Vaccaro, J. P. Lawrence, J. Hong, H. Schellekens, M. H. Alaoui-Ismaili, and D. Falb. Immunogenicity of bone morphogenetic proteins. *J. Neurosurg. Spine* 10:443–451, 2009.

[9]Jiang, H., Y. Hu, P. Zhao, Y. Li, and K. Zhu. Modulation of protein release from biodegradable core-shell structured fibers prepared by coaxial electrospinning. *J. Biomed. Mater. Res. B Appl. Biomater.* 79:50–57, 2006.

[10]Krebsbach, P. H., S. A. Kuznetsov, K. Satomura, R. V. Emmons, D. W. Rowe, and P. G. Robey. Bone formation in vivo: comparison of osteogenesis by transplanted mouse and human marrow stromal fibroblasts. *Transplantation* 63:1059–1069, 1997.

[11]Mundy, G., R. Garrett, S. Harris, J. Chan, D. Chen, G. Rossini, B. Boyce, M. Zhao, and G. Gutierrez. Stimulation of bone formation in vitro and in rodents by statins. *Science* 286:1946–1949, 1999.

[12]Mutsuga, M., Y. Narita, A. Yamawaki, M. Satake, H. Kaneko, Y. Suematsu, A. Usui, and Y. Ueda. A new strategy for prevention of anastomotic stricture using tacrolimus-eluting biodegradable nanofiber. *J. Thorac. Cardiovasc. Surg.* 137:703–709, 2009.

[13]Mutsuga, M., Y. Narita, A. Yamawaki, M. Satake, H. Kaneko, A. Usui, and Y. Ueda. Development of novel drug-eluting biodegradable nano-fiber for prevention of postoperative pulmonary venous obstruction. *Interact. Cardiovasc. Thorac. Surg.* 8:402–406, 2009 (discussion 406–407).

[14]Nagano, M., T. Kitsugi, T. Nakamura, T. Kokubo, and M. Tanahashi. Bone bonding ability of an apatite-coated polymer produced using a biomimetic method: a mechanical and histological study in vivo. *J. Biomed. Mater. Res.* 31:487–494, 1996.

[15]Nakase, T., and H. Yoshikawa. Potential roles of bone morphogenetic proteins (BMPs) in skeletal repair and regeneration. *J. Bone Miner. Metab.* 24:425–433, 2006.

[16]Nie, H., and C. H. Wang. Fabrication and characterization of PLGA/HAp composite scaffolds for delivery of BMP-2 plasmid DNA. *J. Control Release* 120:111–121, 2007.

[17]Nyan, M., D. Sato, H. Kihara, T. Machida, K. Ohya, and S. Kasugai. Effects of the combination with alpha-tricalcium phosphate and simvastatin on bone regeneration. *Clin. Oral Implants Res.* 20:280–287, 2009.

[18]Nyan, M., D. Sato, M. Oda, T. Machida, H. Kobayashi, T. Nakamura, and S. Kasugai. Bone formation with the combination of simvastatin and calcium sulfate in critical-sized rat calvarial defect. *J. Pharmacol. Sci.* 104:384–386, 2007.

[19]Piskin, E., I. A. Isoglu, N. Bolgen, I. Vargel, S. Griffiths, T. Cavusoglu, P. Korkusuz, E. Guzel, and S. Cartmell. In vivo performance of simvastatin-loaded electrospun spiral-wound polycaprolactone scaffolds in reconstruction of cranial bone defects in the rat model. *J. Biomed. Mater. Res. A* 90:1137–1151, 2009.